Geodesy and Geodynamics xxx (xxxx) xxx

Contents lists available at ScienceDirect

Geodesy and Geodynamics

journal homepage: http://www.keaipublishing.com/geog

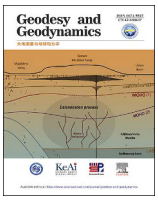

Research Paper

The 1929 Las Malvinas - Villa Atuel earthquake: A deterministic seismic hazard assessment nearly a century later, Mendoza, Argentina

Julián Olivar [a,b,*], Silvina Nacif [a,c], Andrés Folguera [a,b,d]

[a] National Scientific and Technical Research Council (CONICET), Buenos Aires C1033AAJ, Argentina
[b] Faculty of Exact and Natural Sciences, University of Buenos Aires, Buenos Aires C1428EGA, Argentina
[c] F. Volponi Seismological Geophysical Institute, Faculty of Exact, Physical and Natural Sciences, National University of San Juan, San Juan, Argentina
[d] Institute of Andean Studies "Don Pablo Groeber" (IDEAN, UBA-CONICET), Buenos Aires C1428EGA, Argentina

ARTICLE INFO

Article history:
Received 3 February 2026
Received in revised form
5 June 2026
Accepted 11 June 2026
Available online xxx

Keywords:
Seismic hazard
Las Malvinas-Villa Atuel earthquake
San Rafael Block
Deterministic seismic hazard assessment
Seismogenic faults

ABSTRACT

On May 30, 1929, an earthquake with an estimated ~ M_W6.5 caused 30–40 fatalities and destroyed the towns of Las Malvinas and Villa Atuel, in the Andean foreland of Mendoza province, Argentina. This region is characterized by low-rate $M < 4$ crustal seismicity owing to regional compressional stresses that uplift a basement block known as the San Rafael Block. The exact hypocenter and source fault of the 1929 event remain uncertain, with several disagreeing proposals in the literature. Studies based on the classical tectonic framework of an east-vergent uplift place the hypocenter on the proposed west-dipping frontal structure, known as Las Malvinas fault. However, interpretations derived from historical field observations of the damage caused by the earthquake, locate it east of that fault, revealing a major inconsistency between both approaches. Additionally, given nearly a century of urban growth since the historic earthquake, the elements exposed to a comparable event have increased substantially. This work provides a deterministic seismic hazard analysis (using OpenQuake Engine) in the center of Mendoza province by simulating three possible scenarios for the 1929 event, with the goals of i) shedding light on the discussion about the hypocenter location by testing which scenario would better fit both historical damage observations and structural features of the region; ii) finding out the approximate ranges of ground motion that would occur on specific sites of interest; iii) comparing the results with existing large-scale probabilistic studies and current building codes to evaluate possible improvements on risk mitigation in the area. Our results favor a hypocenter located east of the San Rafael Block, matching the historical proposal derived from field observations and reinforcing our alternative tectonic interpretation of a large-scale deep-seated ramp as the main structure driving its uplift, which would be west-vergent instead, together with major seismic activity in the region.

© 2026 Editorial office of Geodesy and Geodynamics. Publishing services by Elsevier B.V. on behalf of KeAi Communications Co. Ltd. This is an open access article under the CC BY-NC-ND license (http://creativecommons.org/licenses/by-nc-nd/4.0/).

1. Introduction

Seismic hazard in the Southern Andes is commonly associated with mega-thrust earthquakes occurring in the Chilean trench, due to the subduction of the Nazca oceanic plate under the continental South American plate. However, in Argentina, this type of earthquake does not pose a major threat due to the distance between its territory and the trench. Instead, smaller but still damaging crustal intraplate earthquakes are the main source of seismic hazard throughout the Argentine side of the Andes, specifically in San Juan and Mendoza provinces [1–5]. Particularly in Mendoza province, the Andean and foreland regions host shallow intraplate seismicity that has caused disasters throughout history. Some examples are (see yellow stars in Fig. 1 for locations): Mendoza city 1861, Mercalli intensity IX-X, destruction of the city and 6000 fatal victims out of 18,000 inhabitants [5–7]; Costa de Araujo 1920, ~M6.7, intensity VIII, destruction of small villages, 250 fatalities, and many more injured [5,8]; Colonia Las Malvinas - Villa Atuel 1929, ~M6.5, intensity VIII, destruction of villages, 30–40 casualties and a great number of injuries [9–11]; Mendoza city

* Corresponding author. National Scientific and Technical Research Council (CONICET), Buenos Aires C1033AAJ, Argentina.
E-mail address: julianandresolivar@gmail.com (J. Olivar).

Peer review under the responsibility of Editorial office of Geodesy and Geodynamics

https://doi.org/10.1016/j.geog.2026.06.001

1674-9847/© 2026 Editorial office of Geodesy and Geodynamics. Publishing services by Elsevier B.V. on behalf of KeAi Communications Co. Ltd. This is an open access article under the CC BY-NC-ND license (http://creativecommons.org/licenses/by-nc-nd/4.0/).

Please cite this article as: J. Olivar, S. Nacif and A. Folguera, The 1929 Las Malvinas - Villa Atuel earthquake: A deterministic seismic hazard assessment nearly a century later, Mendoza, Argentina, Geodesy and Geodynamics, https://doi.org/10.1016/j.geog.2026.06.001

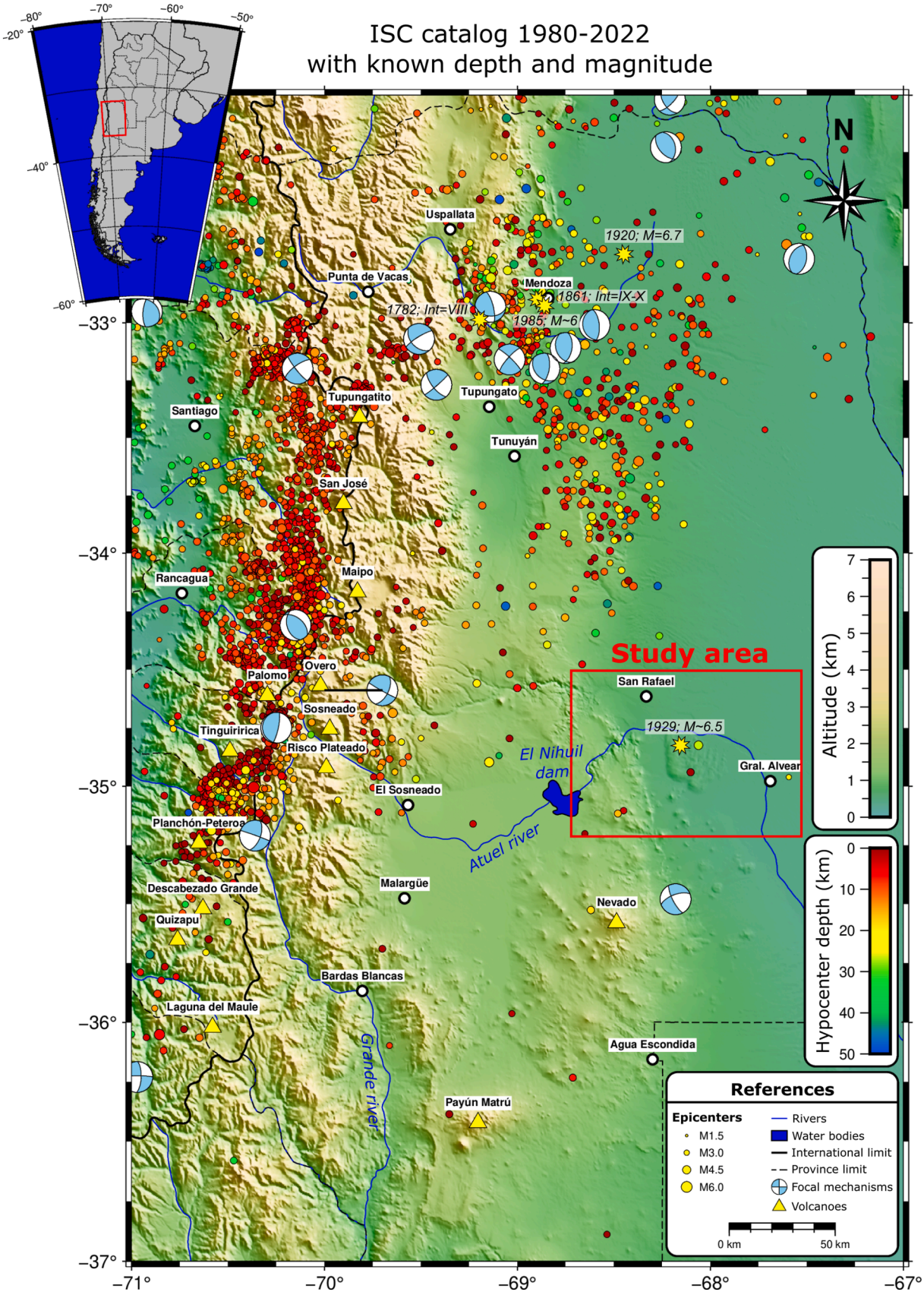

Fig. 1. Topographic map of Mendoza province indicating the study area and crustal seismicity (depth <50 km) from the ISC catalog (ISC reviewed 1980–2022 [15]). Focal mechanisms are taken from the GCMT catalog (Global Centroid Moment Tensor [16,17]). White dots indicate urban settlements, while yellow stars indicate estimated epicenters of historic earthquakes.

1985, $M = 6$, intensity VIII, considerable damage in old buildings and few victims [5,12].

The repeated seismic tragedies suffered in the western region of Argentina encouraged the creation of a national agency that would be in charge of monitoring, studying, and reporting earthquakes, as well as enforcing seismic building codes to mitigate risk. This agency was created in 1944 under a different name, but today it is known as “Instituto Nacional de Prevención Sísmica" (“INPRES”). Until recently, INPRES used to report only a low-resolution, country-scale seismic hazard map [13]. This map divided the national territory into five zones, each with an associated qualitative hazard term (e.g., “low”, “moderate, “high”) and a single value of peak ground acceleration (PGA) with a 10% probability to be exceeded in 50 years. The building codes currently in force were developed based on these values by the same institution (“INPRES-CIRSOC 103” [14]).

In early 2023, INPRES published a new country-wide hazard map with updated information, improved methods, and continuous ground motion values expressed as PGA for a 475-year return period, instead of discrete zones [18–20]. Their study divides the country into 162 smaller seismogenic regions based on international and their own seismic catalogs, as well as some basic information on active faults and local geology. The seismic catalogs come from INPRES's own national seismic network or other regional networks, which many times fail to detect low magnitude earthquakes or carry high uncertainties in hypocenter locations (sometimes assigning arbitrary depths, for example). These data are sufficient for a large-scale assessment but may fall short for local studies. Furthermore, the updated hazard assessment has not been translated into an update of the building codes.

In Mendoza province, INPRES has six seismic stations in the northern region, home to Mendoza city (the capital and biggest city of the province) and focus of most seismological studies. However, for most of the time, it has only had one station in its central region, where studies have been scarce, and which features several $M > 6$ earthquakes in the record. This includes the 1929 Colonia Las Malvinas - Villa Atuel (“LMVA” from here) earthquake [9–11]. Official reports on seismic hazard in that particular area are not thorough and could use a lot of improvement [21]. Although the number of elements at risk in this region is much lower than in the northern one, there are still many small towns and important settlements like San Rafael (which attracts a lot of tourists during summer) and General Alvear cities, and other key infrastructure such as hydroelectric dams that could be at risk of another moderate-big earthquake like the one of 1929. Population growth, urban development, and the increase in economic activities in the area since that year also motivate the need for a renewed and specific risk assessment.

The main goal of this work is to provide a first step into the risk assessment of the area by carrying out a deterministic seismic hazard analysis for different earthquake scenarios in the central region of Mendoza province. We simulate the historic 1929 LMVA event and additional hypothetical cases based on previous seismotectonic studies. This carries three subordinate goals that will contribute to open questions about the study area.

a) Where was the 1929 hypocenter located, and which fault was responsible? For this, a revision of testimonies found in the literature is carried out to reconstruct the hypocenter and magnitude from an estimated macroseismic field. The discussion about the seismogenic fault is aided by previous work on the seismotectonics of the area by the authors, together with additional information from the literature. The former includes locations of low-magnitude earthquakes with data from a local network named “BSR” (“Bloque San Rafael”) [22].
b) What would be the ground shaking in towns, cities, and hydroelectric dams located in the area produced by an event like this, or by a worse scenario? This is tackled using the deterministic hazard calculation tool of the OpenQuake software [23].
c) How do these results compare to existing hazard maps (e.g., INPRES, Global Earthquake Model), and how do they relate to the building codes presently in force in Argentina? This comparison allows, on the one hand, to test the validity of the results, and on the other hand, to provide recommendations on further studies and possible mitigation measures that should be encouraged in the region.

Estimating ground motion fields from earthquake scenario simulations requires thorough research on input parameters. Specific goals involved in this process include recollecting available data on potential seismic sources, seismic catalogs, historical registers and testimonies from the 1929 earthquake, seismic hazard maps, local geology, structure, and anthropic elements. Additionally, research is conducted on soil types to estimate seismic parameters, and on ground motion prediction equations (GMPEs) applicable to the area to aid the scenario-based hazard calculations.

2. Geological and tectonic setting

The study area is located in the Andean foreland region in the center of Mendoza province, Argentina (Fig. 1). The seismotectonic setting is characterized by different morphostructural domains, each with particular geological and structural features, evolution, and present dynamics (Fig. 2). For the specific area that comprises this study, the only relevant domains are the San Rafael Block (“SRB” from here) and the Alvear basin.

The SRB consists mainly of pre-Jurassic basement rocks exhumed in the foreland of the Southern Central Andes, 100 km to the east of the Andean front at around 35°S (Fig. 3) [24,25]. It is located to the south of the Chilean-Pampean flat subduction zone, a very well-known and studied feature of the Andes that produced the uplift of several mountain ranges in the foreland [26,27]. The SRB origin has been associated with another hypothetical shallow subduction configuration, the Payenia shallow subduction zone, developed between 13 Ma and 4 Ma [28]. However, its eastern orogenic front is still associated with contractional neotectonic deformations along the Cerro Negro-Las Malvinas fault and seismic activity, which includes the historic ~ M_W6.5 (estimated) LMVA earthquake that occurred in 1929 (Fig. 3) [9–12,29]. The neotectonic activity in the retroarc zone can be justified based on the transitional geometry between the flat slab to the north and a steeper zone to the south [30,31].

The structure of the SRB is characterized by NNW to NW structures affecting the different Paleozoic-Mesozoic units, conditioned by a lower Paleozoic ductile fabric, derived from the Early Paleozoic deformation and the inversion of Triassic rift systems [29,35,36]. The general vergence of the SRB has been determined to the east based on the description of neotectonic deformation focused on the eastern topographic flank [10–12,29]. However, a recent study of the crustal structure based on the seismicity and gravimetric signal of the block has concluded an opposite vergence (towards the SW) of the main uplifting structure [22]. The study also proposed that the main structure corresponds to one or more blind faults propagating deep into the crust and hosting the deep seismicity whose epicenters are projected eastward of the SRB, where urban settlements are located. This information is relevant for the review of the possible seismogenic

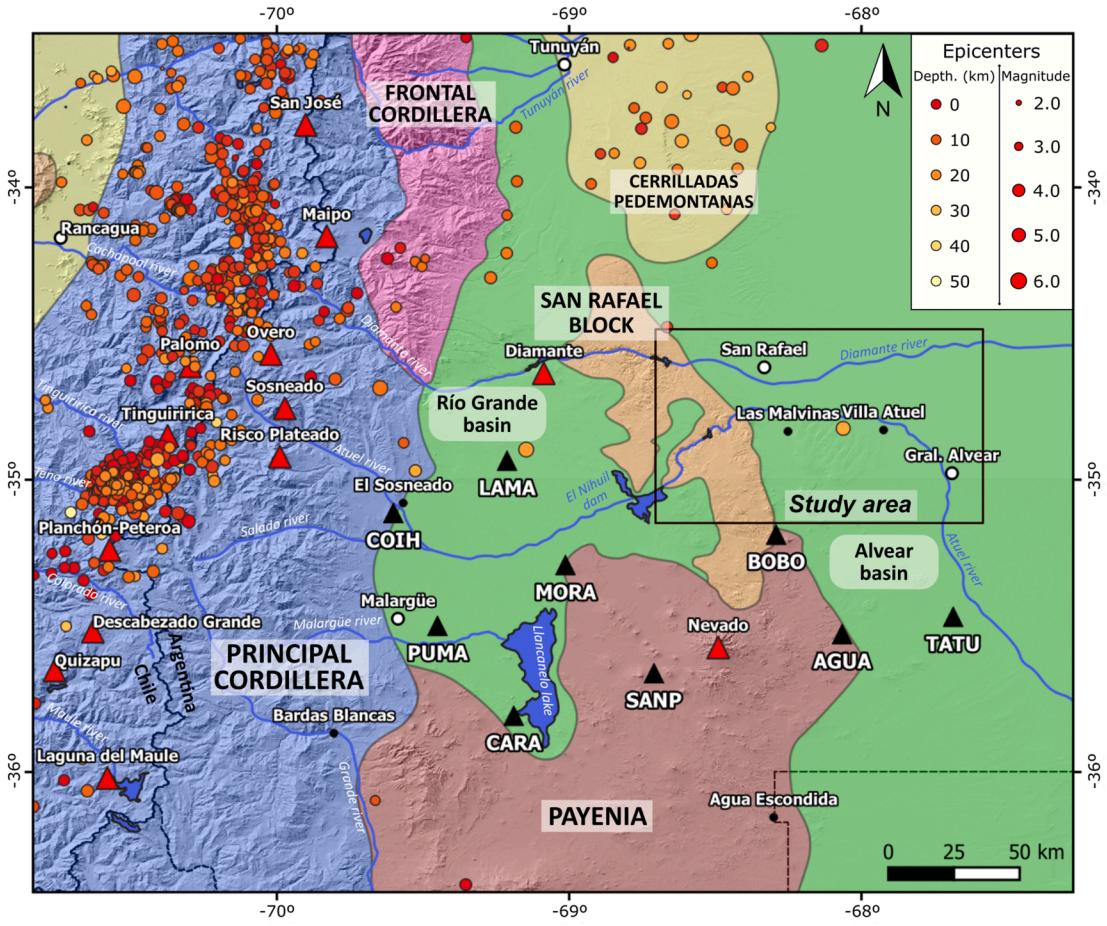

Fig. 2. Context and morphostructural domains of the study area. Black triangles indicate seismic stations of the "BSR" local network. White and black dots correspond to cities and lesser urban settlements, respectively. Red triangles indicate volcanoes. Seismicity is taken from the ISC catalog but shows only records with location errors lower than 10 km in every direction.

structure of the 1929 earthquake, which is one of the main discussion points of this manuscript and will be evoked later on.

Evidence of neotectonic activity has been described in different fault segments within the SRB and surrounding areas (Fig. 3). Among the basement outcrops lie the Aisol fault and the Valle Grande fault [37,38], which feature a straight morphology, NW-SE strike, downthrown blocks on the SW side, and descriptions of scarps with Quaternary displacement. To the east of the SRB, the Santa Isabel fault is found, with a N–S strike, a downthrown block to the west, and a minimum displacement age of 250 ka based on the dating of pedogenic carbonates affected by the fault [39]. However, the most relevant descriptions of neotectonics are situated in the eastern front of the SRB, specifically in the Las Malvinas and Cerro Negro faults. Branellec et al. [11] argued that these are the only faults in the block that show clear neotectonic-morphologic features. They confirmed Pleistocene activity with cosmogenic dating of terraces in the hanging wall (60–80 ka) and assigned the Las Malvinas fault as a possible seismogenic structure of the 1929 historic earthquake (~*M*6.5), as it had been suggested by previous authors [10,12]. They also did estimations on their seismogenic potential based on measurements of the morphologic fault length in different segments, following the Wells and Coppersmith relationships [40], resulting in maximum possible earthquakes of *M*6.3 and *M*6.9 on the Cerro Negro and the Las Malvinas faults, respectively. Finally, they included an estimation of the recurrence time of such an event based on their slip rate calculations, which resulted in 440 years for the former and 520 years for the latter. These are key pieces of information in the discussion about the hypocenter and magnitude of the 1929 event.

The ongoing tectonic activity in the region is also expressed as crustal seismicity with a depth lower than 40 km. However, international catalog records are scarce and possess high completeness magnitude. Specifically in the study area, it is clear from Figs. 1 and 2 that seismicity is almost absent from the ISC records. The catalog built by INPRES from their national seismometer network does not report hypocentral location errors and, given that they only count on one station near the area, the precision of the locations would be weak. The main source of knowledge on the seismicity distribution are studies based on local and temporary networks, which have not been uploaded to said catalogs but are available in the literature [22,41] (Fig. 4). These studies have mostly recollected low-magnitude seismicity (below *M*4), since the time span of the local networks has not been long enough to capture high-magnitude events. The details on hypocenter location parameters, uncertainties and overall quality are shown and discussed in the respective cited papers. An interesting feature that was unveiled by these studies is the deep (20–30 km) seismicity located eastward of the SRB front, which, as mentioned before, was interpreted (also using gravimetric data) as the activity of blind faults with a strike following the structural tendency of the region (Az ~330°) and dipping to the northeast ([22], Fig. 9 therein). These would be crustal-scale faults that

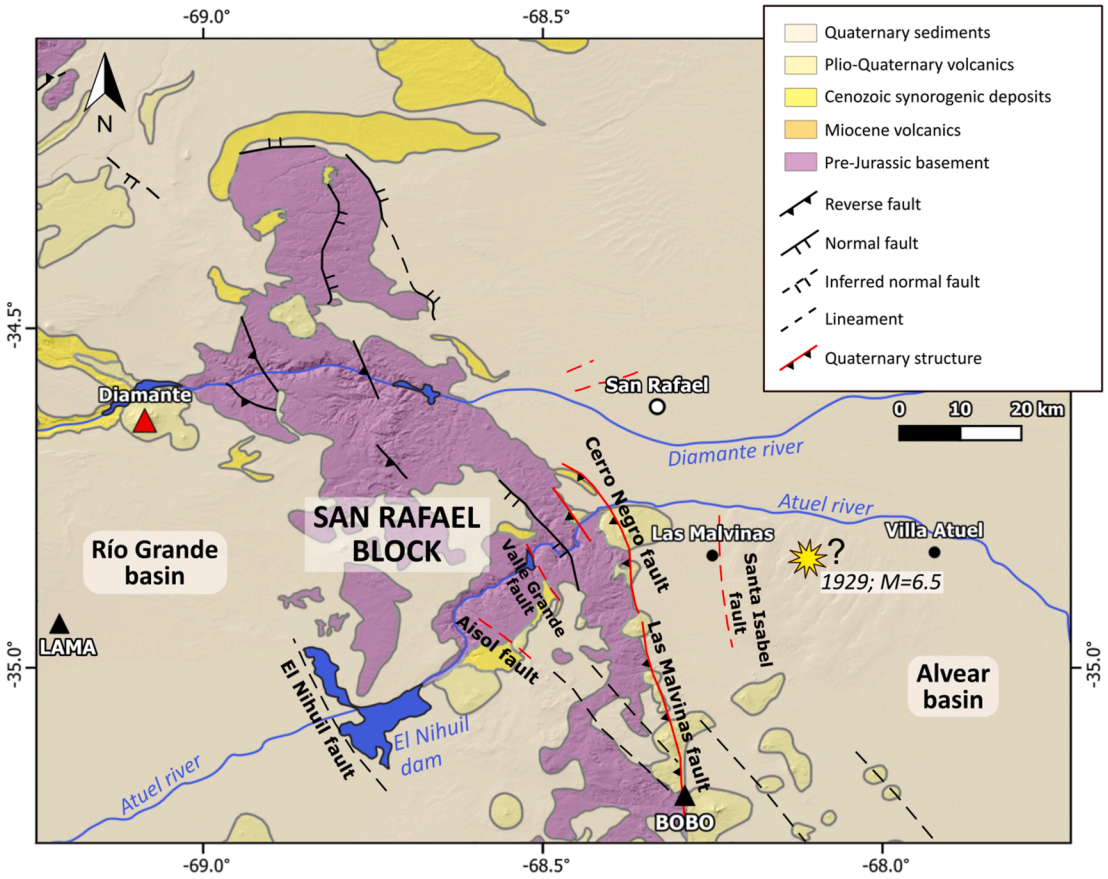

Fig. 3. Simplified geological map of the San Rafael Block area, including structures and indicating those with neotectonic activity in red (based on [32–34]). The yellow star indicates the approximate location of the historic Villa Atuel-Las Malvinas earthquake (the exact epicenter is unknown). Other symbols are as in Fig. 2.

extend northward as well, below the most populated area around San Rafael city.

3. Background on seismic hazard and elements at risk

Near the SRB the last $M \geq 6$ earthquake was the 1929 LMVA event, whose exact hypocenter is still under discussion. There are discrepancies between many possible hypocenters estimated to be eastward of the SRB according to the damage caused, and a potential hypocenter hosted in the Las Malvinas fault which dips in the opposite direction (Fig. 4). The earthquake caused between 30 and 40 fatalities (depending on the source) and destroyed Las Malvinas and Villa Atuel towns almost completely, as well as causing lesser damage to other nearby settlements. It was also felt in numerous sites of bordering provinces (San Juan, San Luis, Neuquén), and even up to Olavarría in Buenos Aires province (745 km away to the east) [9].

There are no specific seismic hazard studies that focus on this area, but there are hazard estimations that come from global or country-scale studies. The global study corresponds to the Global Earthquake Model ("GEM") hazard map, which is calculated for reference rock parameters (Fig. 5a [42]). As mentioned before, the country-scale maps were composed by INPRES (Fig. 5b). Both sources agree on a 10% probability in 50 years to exceed values of PGA in the range of 0.15–0.35 g, but each has a very different distribution on the map.

Another important aspect for the seismic hazard analysis is the ground composition. At a broad scale, the area is characterized by two distinct zones: the western region is dominated by the low-relief SRB rock outcrops of the pre-Jurassic basement, intertwined with small pockets of low-thickness Quaternary sediments. To the east, the landscape is covered by Quaternary sediments, mostly fluvial and some of aeolian origin [32]. Their composition is generally dominated by sand with lower proportions of silt and clay (sandy loam soils [43]). Analysis of samples taken from Salto de las Rosas and 25 de Mayo (see Fig. 4 for locations of these towns) showed compositions of 67.5% fine sand, 22.5% clay, and 10% silt [44]. This is relevant for the present study since it will serve as a proxy for classifying the soil in terms of its seismic parameters. Published data on seismic parameters and site effects specifically for this area are scarce, being mostly focused in northern Mendoza province instead [45].

The main urban settlements in the area are two small cities: San Rafael and General Alvear (Fig. 4). Census data from 2010 reported 120 thousand inhabitants in the former and 30 thousand in the latter. Around both cities, there are areas occupied by scattered houses, and, mainly following the two main rivers (Diamante and Atuel), agricultural activity has led to the development of large farming fields where occasional buildings are found. There are also several towns like Villa Atuel, Colonia Las Malvinas, Salto de las Rosas and Goudge, among others, serving as nuclei of those agricultural fields. Following the Atuel river valley inside the SRB, there are scarce buildings mostly related to touristic activities and a hydroelectric dam known as the Valle Grande dam. Other dams in the area include the El Nihuil dam in the Atuel river, and the Los Reyunos dam in the Diamante river (Fig. 4).

Even though national census data from 2022 is still not fully available, there are provisional results reported at a department

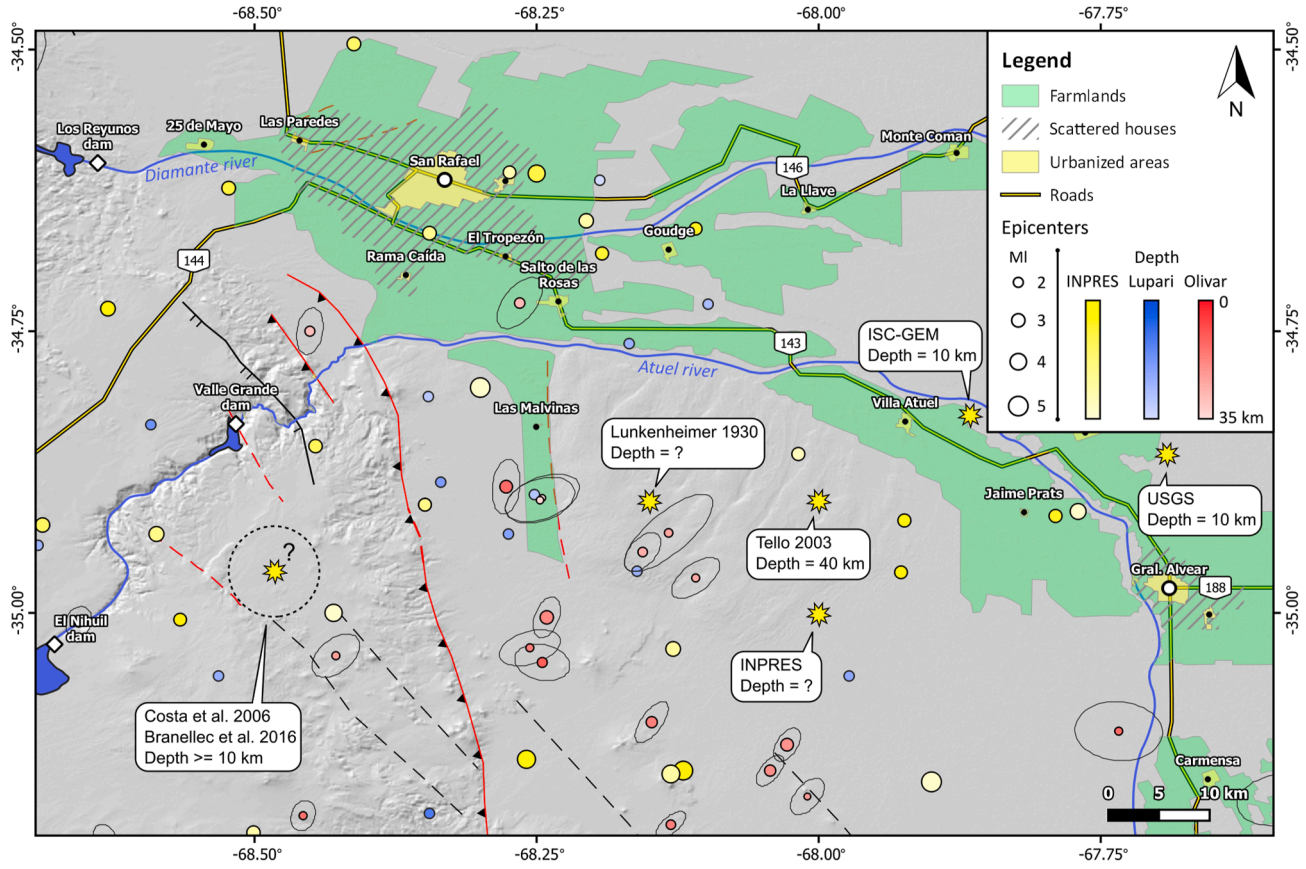

Fig. 4. Seismicity located with regional (INPRES) and local networks [22,41], suggested epicenters for the 1929 LMVA event by different authors (yellow stars), and anthropic elements. Seismicity by Lupari et al. [41] does not report magnitude; size on the map is fixed. Ellipses around seismicity by Olivar et al. [22] indicate location errors with a 68% confidence level. Structures and other symbols are as in Fig. 3.

scale, a second-tier political division of provinces. Most of the study area is located in the San Rafael department, which according to the last census, had 209,068 inhabitants and 82,865 households (it does not report the number of buildings). It is important to note that most of the population of this department is concentrated in the study area (probably over 90%) since there are no other cities and only a few towns outside of it. The same happens with the Alvear department, where General Alvear city is located, and which reported 49,930 inhabitants and 20,108 households. Still, the population density in the area is very low, so the main focus for hazard calculations will be made on specific settlements and hydroelectric dams.

4. Methodology and simulation parameters

The workflow of this study included the following steps: research, mapping, testing parameters for earthquake scenario simulations, modeling with OpenQuake, processing and generating graphic outputs, analyzing and comparing results.

Simulating coherent earthquake scenarios for this particular setting posed a series of challenges. On one hand, since almost a century has passed since the LMVA earthquake, there is scarce instrumental information, and most of what is known comes from descriptions of the disasters that were caused. Some of the descriptions included an estimated macroseismic intensity according to the Modified Mercalli scale, but most of them did not. In those cases, intensity was estimated by defining the damage grade and vulnerability classes of the buildings according to the guidelines of the European Macroseismic Scale 1998 (EMS-98 [46]). On the other hand, simulating earthquake scenarios with OpenQuake requires a certain set of parameters to describe the source (epicenter location, depth, magnitude, fault strike, dip, and rake), attenuation, and site conditions to increase the soundness of the model. Thus, research on GMPEs, soil types, and estimation of seismic parameters were also key parts of the process.

The large number of possible parameter combinations for an earthquake scenario was reduced through research on plausible values. Some parameters had to be fixed to a single value to narrow down the scenarios, and others were tested within limited options (GMPEs, depth, dip, and Vs30).

4.1. Source parameters

Magnitude: the scenarios were computed taking into account the "MHE" (Maximum Historical Earthquake) as the controlling earthquake. The MHE is the 1929 LMVA event, whose magnitude is uncertain but most estimations point towards M_W6.5 ([2,10]; USGS-NEIC catalog; ISC-GEM catalog 6.7 ± 0.3). Since one of the main goals was to reproduce this earthquake, lower magnitudes were not considered and this was the fixed value used for the simulations.

Fault geometry: these parameters include the strike, dip and rake of the fault. They were constrained according to the seismotectonic setting. Strike was defined by the tested seismogenic fault scenarios, generally following the NW structural trend of the region. Rake was fixed at 90° in order to evaluate pure inverse faulting mechanisms, given the contractional tectonic regime [10,11,47]. Including the possibility of a strike-slip component

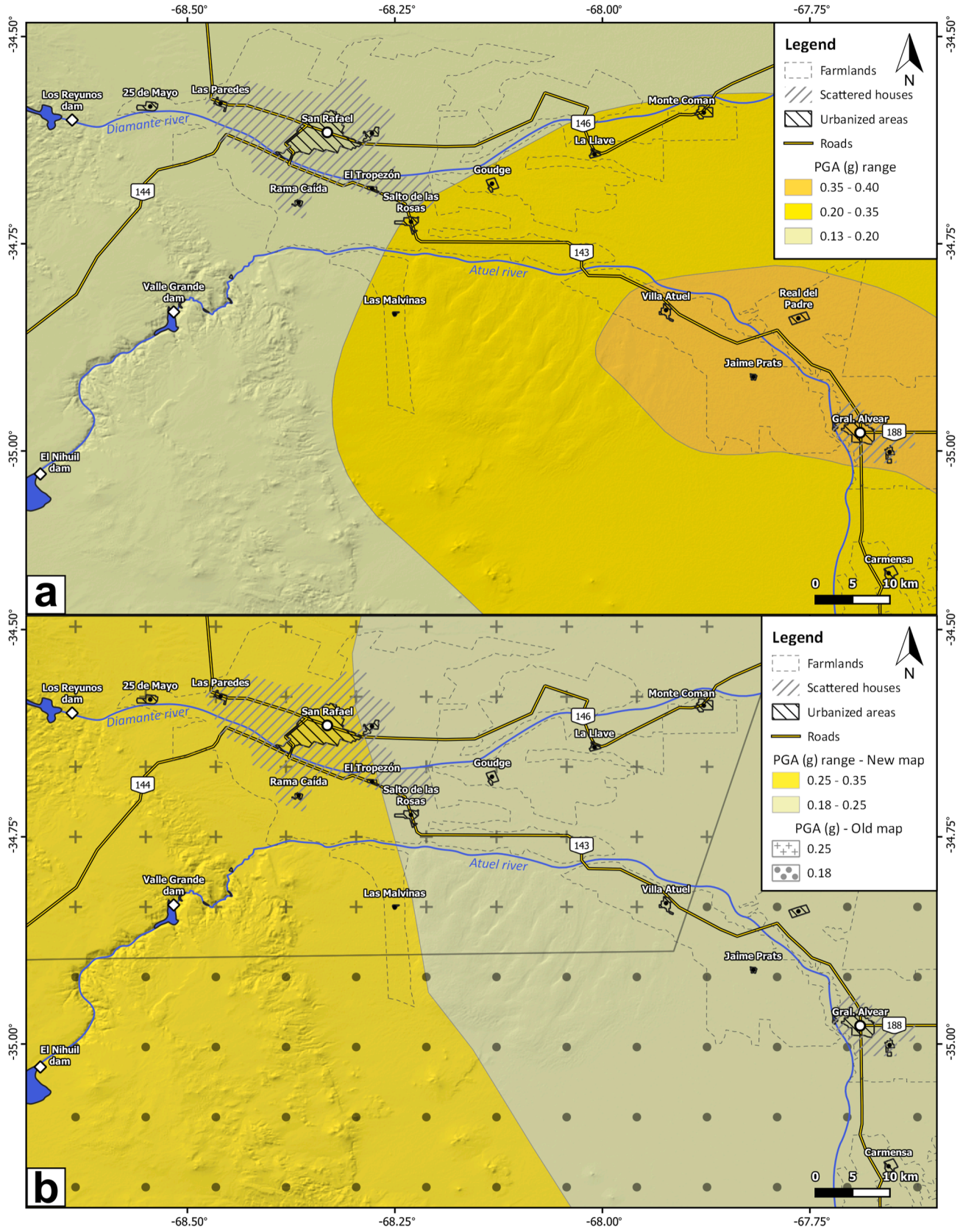

Fig. 5. PGA with a return period of 475 years for the study area according to GEM (a) and INPRES's old and new maps (b).

would over-complicate the analysis, and the results would not change considerably. Inverse faults develop with a lower angle than strike-slip and normal faults, hence, simulated fault dips were relatively low, between 20° and 45°.

Hypocenter location: three seismogenic fault scenarios were tested, as described below. In all three cases, the horizontal distance between the epicenter and the fault's surface trace was calculated trigonometrically, taking into account the fault dip and the possible hypocenter depths (for example, a 35° dip fault and a 10 km deep hypocenter implies an epicenter 14.3 km away from the fault trace).

Scenario A) 1929 LMVA event, assuming it was hosted in the Las Malvinas fault, as suggested by Costa et al. and Branellec et al. [10,11]. To test this hypothesis, an epicenter west of the Las Malvinas fault northern segment was selected, following trigonometric calculations related to the possible depth and dip of the fault (Fig. 6). Costa et al. [10] estimated a 16 km decollement for this fault, while Branellec et al. [11] propose that the hypocenter must have been at least 10 km deep, given that the maximum intensity reported was only VIII and the earthquake was felt in a vast area throughout the country. There are no estimations of the fault dip, but low values combined with a depth greater than 10 km would mean an epicenter too far west from the affected area. Possible dip values were set between 30° and 45°. Likewise, a depth of around 16 km would mean a very high fault dip, which is unlikely for inverse faults. The tradeoff between these parameters led to fixing the hypocenter at 10 km depth and testing different dip values inside the given range. Finally, the strike was set at 170° following the orientation of the fault and the right-hand rule.

Scenario B) The alternate hypothesis supported by other authors and catalogs [2,5,8,9], based on the recorded damage distribution, is that the 1929 LMVA event nucleated somewhere to the east of the SRB (Fig. 4). Following the seismicity depth and the geometry of blind faults beneath this region proposed in Olivar et al. [22], the testing depth range was set to 20–30 km and the dip range to 20°–45°. Strike was fixed at 330° to reproduce a NW-trending fault dipping to the NE. Given the large discrepancies among authors regarding the epicenter, it was constrained by composing an estimated macroseismic field by converting damage descriptions found through research into intensity values, following the guidelines in the EMS-98 [46]. However, in some cases, this procedure was not straightforward; thus, a preliminary relative scale with three levels was defined and plotted (Fig. 6). A summary of the descriptions found in the literature and online newspaper articles is presented in Table 1.

Lunkenheimer [9] also described perturbations in the old railway lines running between Villa Atuel and Monte Coman (mostly focused near Villa Atuel), and the line between Salto de las Rosas and Goudge (see Fig. 6 for locations). In some sites, building damage was described by Lunkenheimer as “slight” and “regular”, which could be translated into intensities between V-VI and VI-VII, respectively. In Las Malvinas and Villa Atuel towns, following the EMS-98 guidelines, the collapse of vulnerability Class A buildings (masonry) implies a damage Grade 5, so that we estimate an intensity closer to IX rather than what INPRES defined as VIII.

According to these descriptions and specifically taking into account the low intensity in General Alvear city, the epicenters displaced to the east reported by ISC-GEM and USGS (Fig. 4) were

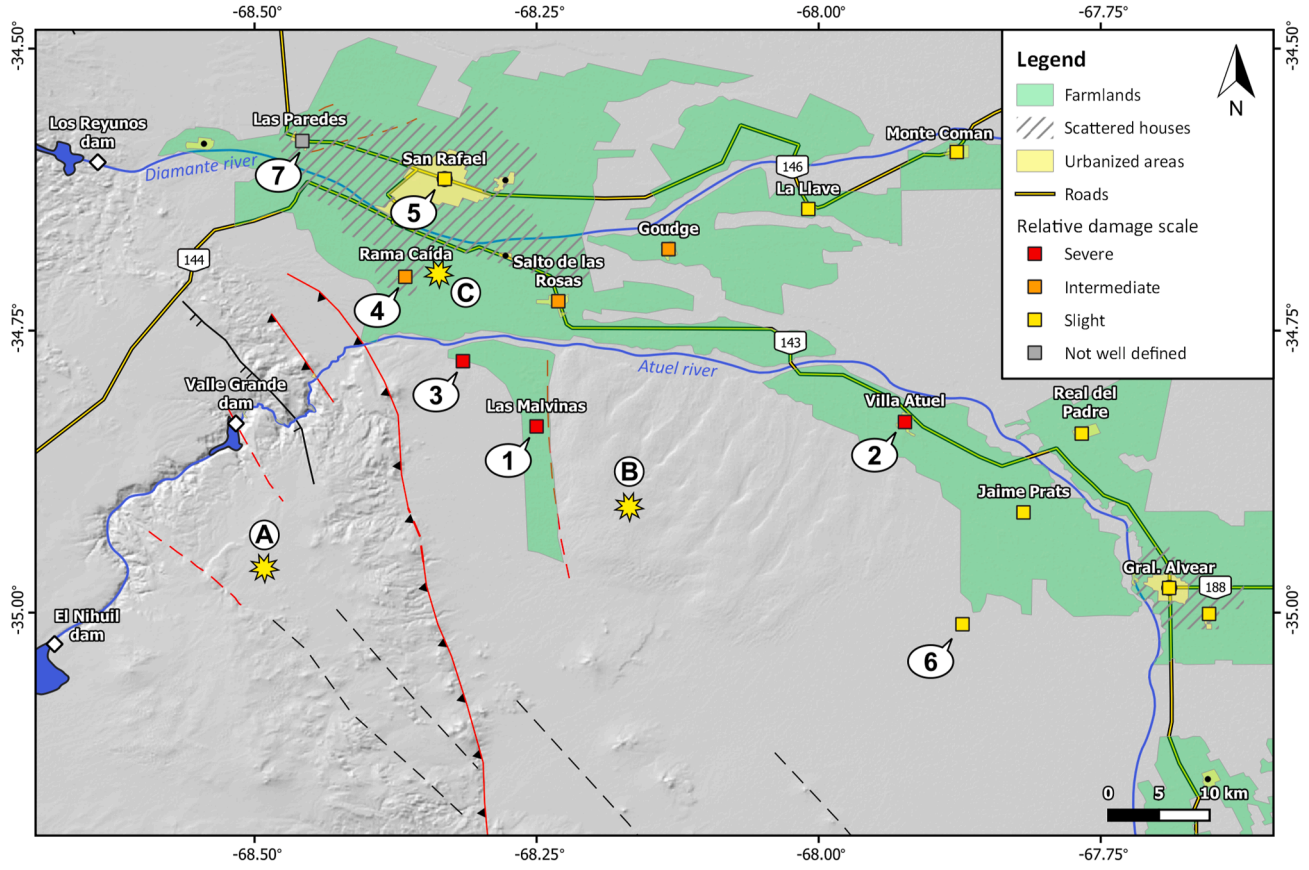

Fig. 6. Epicenters chosen for each of the three scenarios (yellow stars) and sites with descriptions of the 1929 LMVA event effects (squares), linked by numbers in white balloons to Table 1. Sites without numbers were only described as “slight” or “regular” building damage by Lunkenheimer [9]. Structures and other symbols are as in Fig. 3.

Table 1
Descriptions of the effects of the 1929 LMVA earthquake and intensity estimated in this work according to EMS-98 [46].

No	Site	Descriptions	Sources	Int.
1	Las Malvinas	Most buildings are masonry houses made of sandy loess, 5 m high in average. Very large number of almost to completely destroyed houses. 23 fatalities and 31 injured. Some lesser cracks on the ground following house wall directions.	Lunkenheimer, Tello [2,9]	VIII-IX
2	Villa Atuel	Same type of buildings as Las Malvinas, but some made of brick and better cement. Most masonry houses were destroyed, some brick houses severely damaged, and the most resistant ones suffered lesser damage. 17 fatalities out of 900 inhabitants. Ground cracks several meters long and around 4 cm wide. Warm water sprang from cracks and sand/mud craters, some during 4 hours. Liquefaction attributed to a shallow phreatic level at 1 m depth due to irrigation water blocked by clay/basaltic level. Steep decrease of damage, cracks and mud craters along distance from the town center.	Lunkenheimer, Tello, Saurina et al. Izuel [2,9,48,49]	IX
3	El Escorial	"One of the mainly affected sites"	Tello [2]	>VI
4	Rama Caída	"Our big house suffered a lot of shaking and cracking, eight people ran away."	Izuel [49]	V-VI
5	San Rafael	Cracks in some houses.	Izuel [49]	V
6	Soitué	Lesser cracks in buildings of low resistance.	Lunkenheimer [9]	V
7	Las Paredes	A family reports that their house collapsed, but there is no further information or sources.	Izuel [49]	?

discarded. Locations reported by INPRES and Tello [2,5] are displaced to the SE with respect to localities that suffered severe to intermediate damage as Las Malvinas, El Escorial, Rama Caìda, and Salto de las Rosas, which also do not report liquefaction phenomena. We considered the epicenter proposed by Lunkenheimer [9] as the best for the scenario simulation, because it would be easier to justify the serious damage in Las Malvinas with a closer epicenter than in Villa Atuel, where liquefaction could have been the main cause behind the disasters. This last point is also supported by the fact that moving away from Villa Atuel, the damage and mud craters rapidly fade, indicating a very site-specific effect. It is also worth noting that Lunkenheimer did not estimate the source depth, so it was still a parameter to test for this scenario.

Scenario C) The deep seismicity beneath the area near San Rafael city, recorded with local networks (Fig. 4) and gravimetric data [22,41], allows suggesting that the seismogenic deep blind fault proposed in Scenario B also extends to the NW of that epicenter. In this case, a source within the same depth (20–30 km), dip angle (20°–45°), and strike (330°) was modeled, but with an epicenter closer to San Rafael city in order to test a scenario with worse consequences (Fig. 6).

4.2. Attenuation parameters

The next key element in a deterministic hazard analysis are the ground motion prediction equations (GMPEs), which describe how the ground shaking is attenuated with distance from the epicenter. A selection of coherent GMPEs was picked from previous hazard studies in surrounding regions [20,45,50] and in active crustal regions ("ACRs") in general [51].

Research led to a progressive reduction into three GMPEs to be tested. The initial list was taken from INPRES's work on the new hazard map [20], which includes GMPEs by Abrahamson et al. Boore et al., Campbell and Bozorgnia, Chiou and Youngs, and Idriss [52–56].

Similar versions of all of these, except for Idriss [56], are mentioned by Stewart et al. [51] as the most often tested models for ACRs. The compatibility of the models with the scenarios of interest was analysed in view of the GMPE compendium by Douglas [57], to check if they fit in terms of tectonic regime, fault type, magnitude, depth, and soil type, among others.

Of the five models considered, three were carried forward to the testing stage. Campbell and Bozorgnia [54] was discarded since it applies to hypocenters less than 20 km deep. Next, we decided to discard Boore et al. [53] due to inconsistencies reported by INPRES [20]. Chiou and Youngs [55] was the preferred choice by Stewart et al. [51] over the others. On the other hand, Rodriguez [50] used Abrahamson et al. [52] for their hazard study in Neuquén province, bordering Mendoza province to the south and with similar geographic and soil characteristics. Hence, these last two and Idriss [56] were the models chosen for testing.

4.3. Site conditions

The final component required for seismic hazard simulations is the characterization of site effects, which describe how ground motion is amplified or attenuated in specific areas depending on local ground conditions. The possible GMPEs chosen for the simulations consider site conditions based on one or more out of three seismic parameters: Vs30 (average S wave velocity in meters per second of the first 30 m of ground depth), *Z*1.0 (depth in meters to a level with S wave velocity of 1 km/s, also known as "engineering rock") and *Z*2.5 (depth in kilometers to a level with S wave velocity of 2.5 km/s, also referred to as "hard rock") (e.g. Ref. [58]). Because no local studies report these values, they had to be estimated.

For Vs30, there are accepted ranges for different soil compositions divided into categories. Harder soils imply higher velocities. The building codes in Argentina [14] use the soil categories A to F, with the same Vs30 ranges, recommended by NEHRP (National Earthquake Hazards Reduction Program, USA). In this study, since soil types are quite homogeneous, only two regions with different soil conditions were defined, namely "rock" in the areas corresponding to the SRB and "soil" in the areas covered by Quaternary sediments. Studies on local soils were used as a proxy for Vs30 estimations [44]. These were compared to estimations of Vs30 based on high-resolution topographic data (Fig. 7), under the hypothesis that harder rocks and soft soils are associated with the development of high and low slopes respectively, so that the slope becomes a proxy for Vs30 [59–61].

Given that the rock sites of interest include hydroelectric dams, we took a conservative approach, using the value on the lower end (760 m/s, reference rock value). Soil sites were assigned to type D of the NEHRP classification, based on the characteristics described

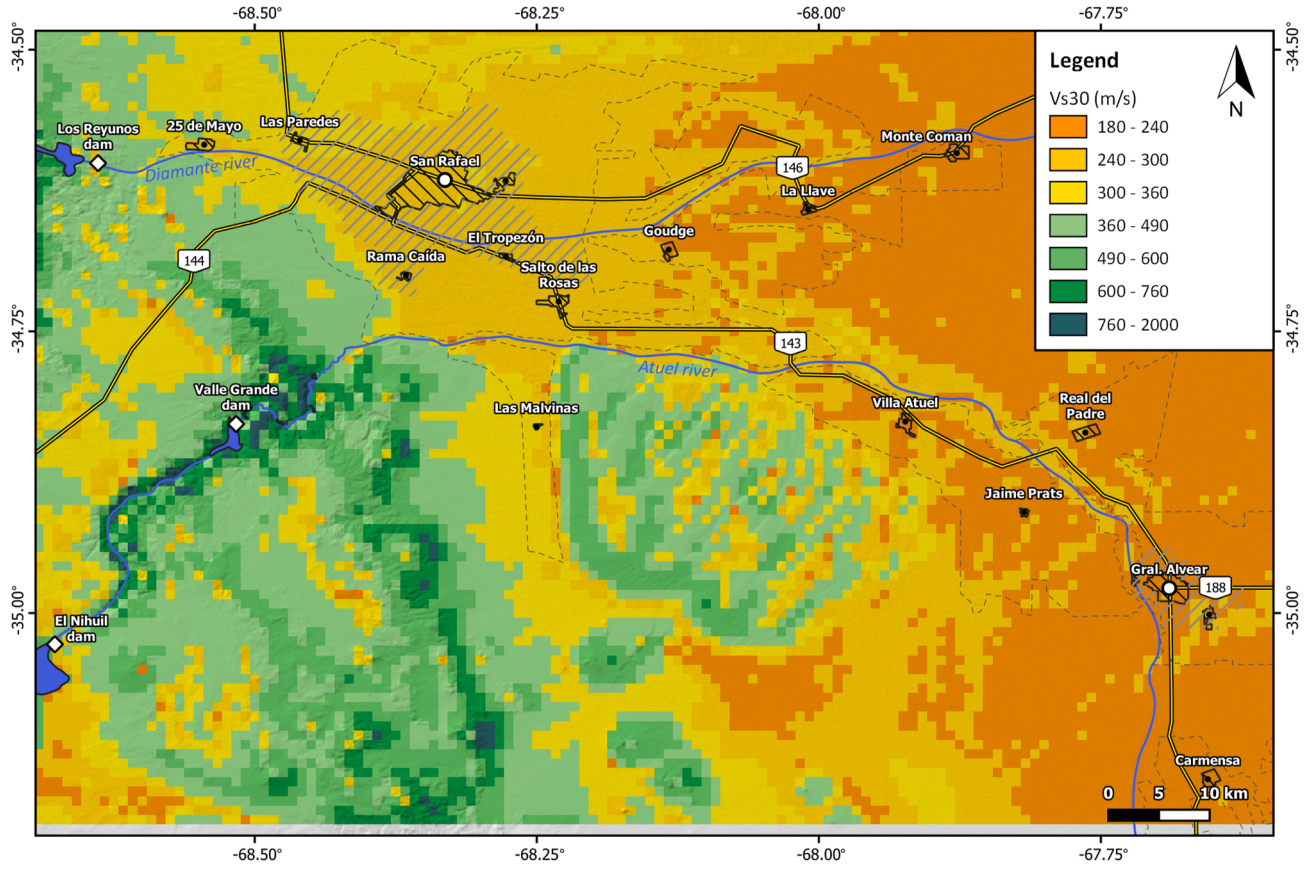

Fig. 7. Vs30 (m/s) estimated from high-resolution topographic data according to the USGS's repository (https://earthquake.usgs.gov/data/vs30/- last visit in December 2025).

in Section 3 of this paper. These present Vs30 values between 180 and 360 m/s according to their variation in finer and coarser material. The fact that soils in the area are dominated by sand rather than silt or clay would preclude values on the lower end. In addition, estimations based on topography (Fig. 7) show that most of the urban settlements lie in areas within 240 and 360 m/s. Then, three values were assigned for testing: 240, 300, and 450 m/s. The last one was intended to evaluate how the results would change if Vs30 estimations were highly underestimated.

Finally, for $Z1.0$ and $Z2.5$ (which not all GMPEs need), OpenQuake provides a tool to estimate them from the Vs30, based on the relationships published by Chiou and Youngs for $Z1.0$ and Campbell and Bozorgnia for $Z2.5$ [54,55].

4.4. Parameter testing with eGSIM

Further filtering of the simulation parameters was done by testing the influence of their variance on the resulting PGA estimations. Tests were carried out using the eGSIM tool by GFZ Potsdam [62], which allows comparing the attenuation predicted by a large list of available GMPEs according to different source and site conditions.

Nine combinations of dip, depth, and Vs30 were tested, each with the three selected GMPEs (see detailed parameters in Fig. 8). The results showed a minor influence of varying depth and fault dip within the established parameters. Most models from "a" to "f" (Fig. 8) show peak values between 0.3 and 0.4 g; and 0.2 g at around 30 km distance with GMPEs by Chiou and Youngs and Abrahamson et al. [52,55]. Hence, the middle point was chosen for scenarios B and C: depth = 25 km; dip = 30°.

The different soil Vs30 values that were tested also showed minor effects in PGA for those two GMPEs. The same tendency of 0.2 g at 30 km distance is observed. Hence, we also selected the middle value of 300 m/s. Note that the value used for rock (760 m/s) does show a clearly lower PGA curve with respect to the rest.

Finally, among the three GMPEs that were tested, Idriss [56] showed the highest variability when assigning different values to the other parameters, as well as the lowest PGA values. Apart from that, this model is recommended for Vs > 450 m/s. As a conservative choice, it was discarded. The other two are very similar, but the final decision was to use Chiou and Youngs [55] due to a better performance according to Stewart et al. [51]. In summary, model "b" shows the final values for soils, while model "i" does for rock.

4.5. OpenQuake simulations

The final input parameters for each scenario simulation were fed into the OpenQuake Engine software to define the earthquake rupture models and calculate the ground motion fields in PGA. The rupture geometry is calculated by the software from the input magnitude, hypocenter, strike and dip using the Wells and Coppersmith relationships [40]. Ground motion fields were calculated both for mapping median PGA over the whole region (with a grid spacing of 1 km) and for the complete PGA Gaussian distribution in seven specific sites following 1000 realizations with intra-event variations inside three standard deviations. The sites correspond to the three hydroelectric dams (Nihuil, Reyunos and Valle Grande), two cities (San Rafael and General Alvear) and two towns (Las Malvinas and Villa Atuel).

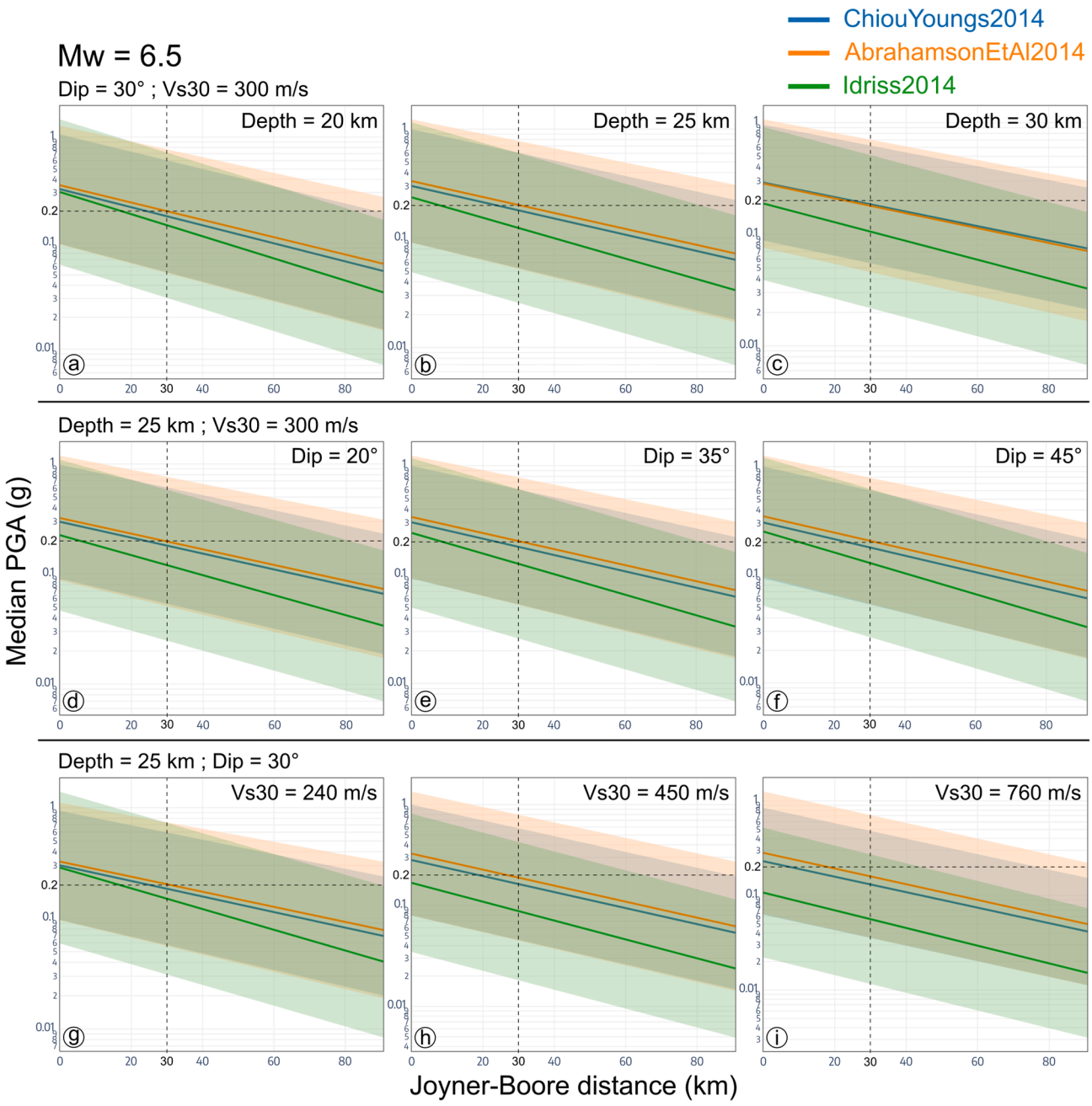

Fig. 8. Attenuation according to different parameter combinations plotted with eGSIM by GFZ Potsdam [62]. Shaded areas show the standard deviation associated with each GMPE.

5. Results

Below we present the results obtained for each scenario in figures that contain: i) the ground motion fields expressed as median PGA shown in maps; ii) the intra-event PGA distribution at the seven sites of interest as box and whisker plots; iii) the statistical summary of each distribution as tables.

Scenario A: The median PGA map shows peak values between 0.25 and 0.37 g concentrated in a 20 × 10 km rectangular area west of the Las Malvinas fault, which expands further on the eastern side where Vs30 drops to soil values (Fig. 9). The attenuation is strong, so that the furthest sites present very low PGA (e.g., Gral. Alvear). Comparing the PGA distribution across 1000 realizations, it can be seen that the most affected site of interest would be the Valle Grande dam, consistently.

Scenario B: In this case, due to the increased source depth, the peak values are lower than in Scenario A, but the attenuation is weaker (Fig. 10). The four urban settlements of interest would be affected by a median PGA greater than 0.15, consistently higher than in Scenario A. On the contrary, the dams present relatively low median values.

Scenario C: The shape and attenuation of the ground motion field are the same as in Scenario B, since the only difference is the epicenter location (Fig. 11). Here, San Rafael city and nearby towns lie inside an area with a median PGA close to 0.3 g. The dams, favoured by higher Vs30 sites, would still suffer lower ground shaking than in Scenario A, with a median below 0.2 g. Finally, PGA at the furthest urban settlements of Villa Atuel and Gral. Alvear would be quite lower than in Scenario B.

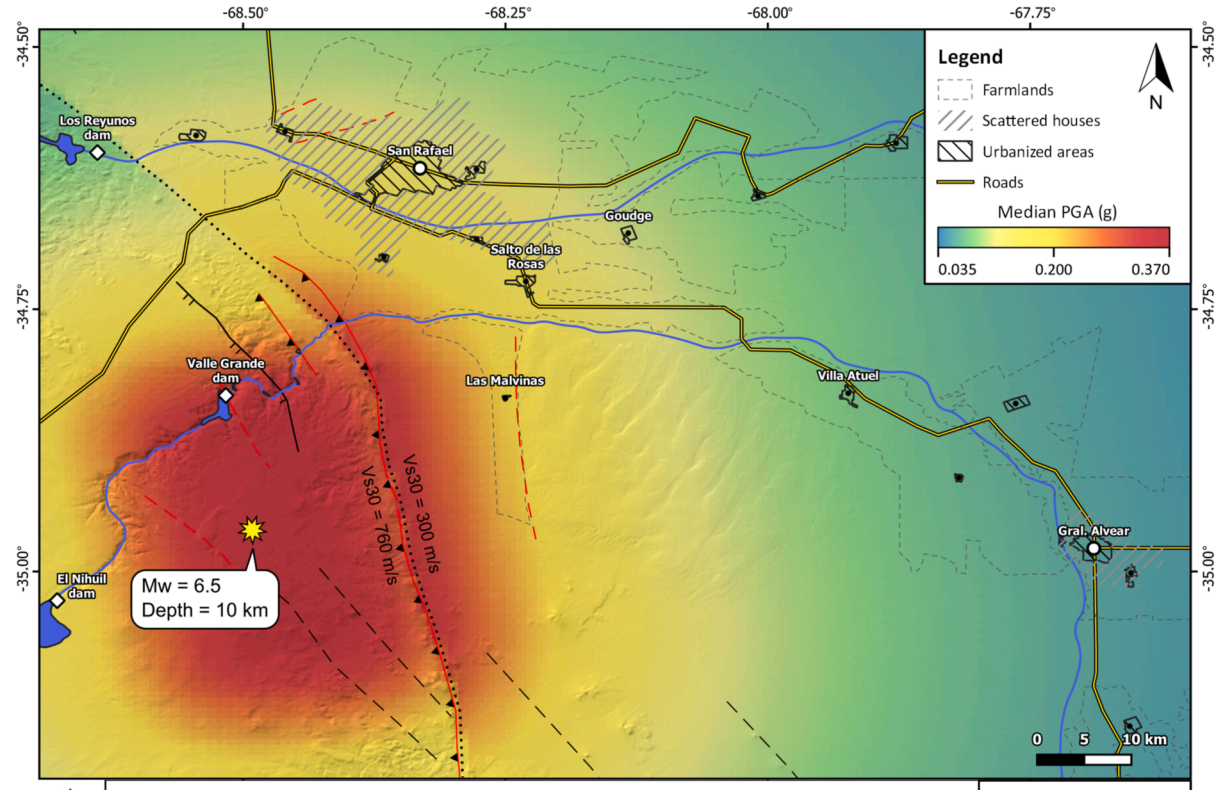

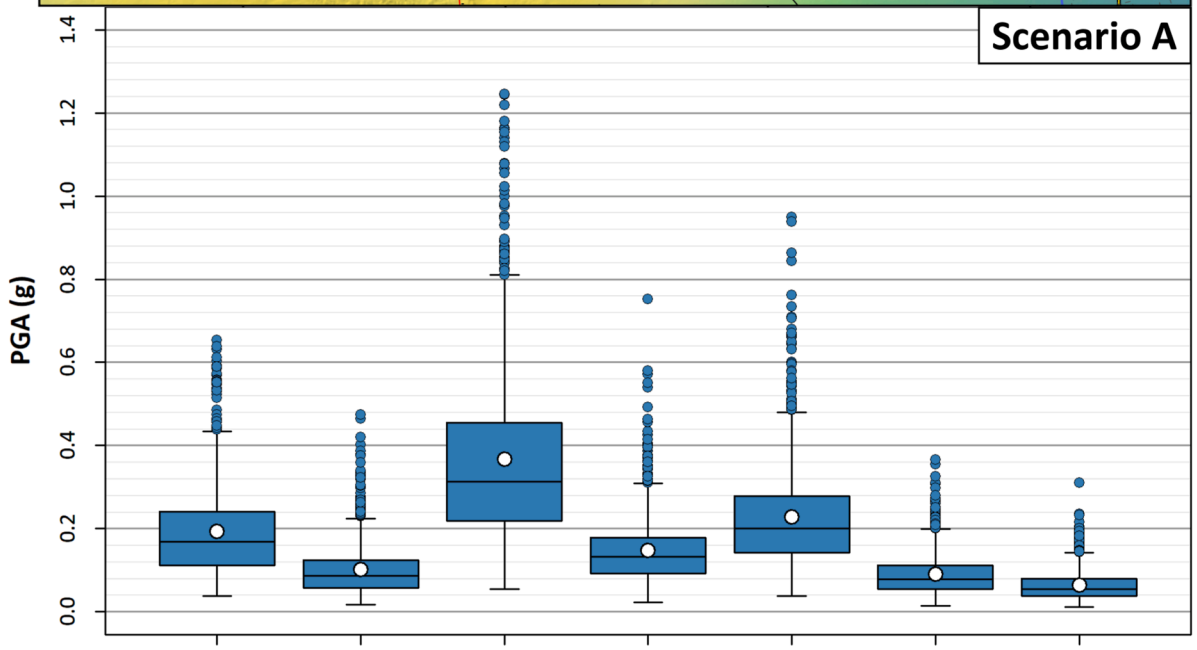

PGA (g)	Nihuil	Reyunos	Valle Grande	San Rafael	Las Malvinas	Villa Atuel	Gral. Alvear
Mean	0.193	0.101	0.368	0.148	0.228	0.091	0.064
Std. dev.	0.111	0.064	0.215	0.081	0.124	0.052	0.037
*Q*1	0.111	0.057	0.218	0.092	0.142	0.054	0.038
Median	0.168	0.086	0.313	0.133	0.200	0.078	0.055
*Q*3	0.241	0.124	0.455	0.179	0.278	0.112	0.080

Fig. 9. Ground motion field for Scenario A expressed as median PGA (g) and anthropic elements. Below, PGA variability for 1000 realizations with a 99% confidence level in the seven sites of interest, with its corresponding summary table.

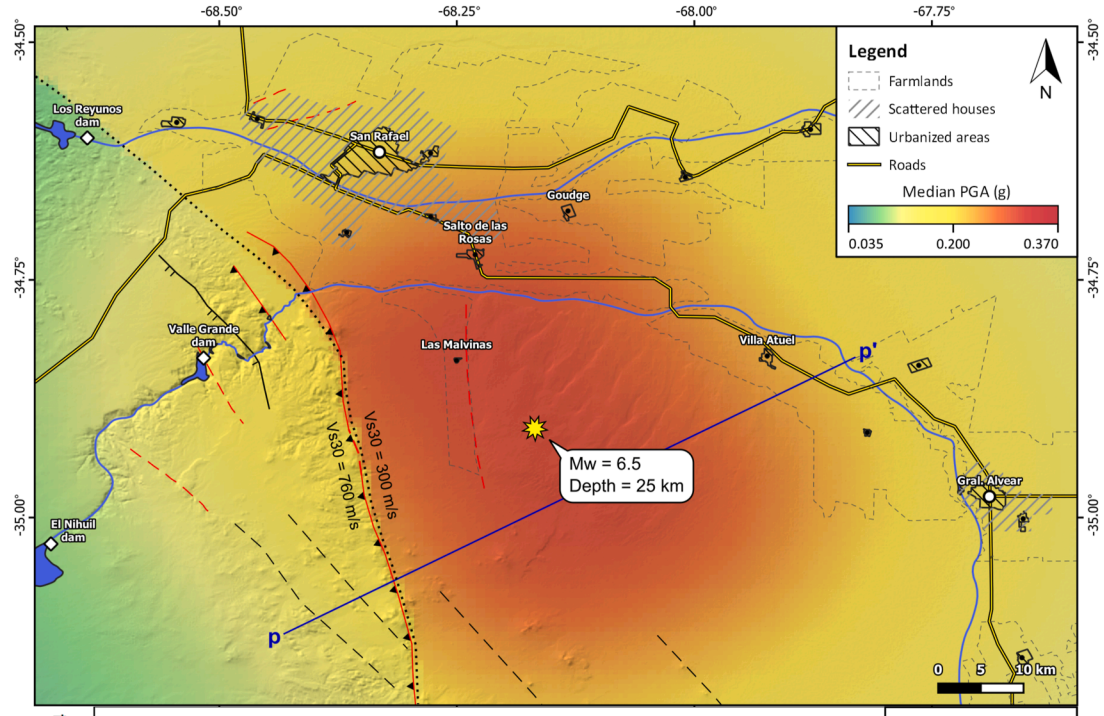

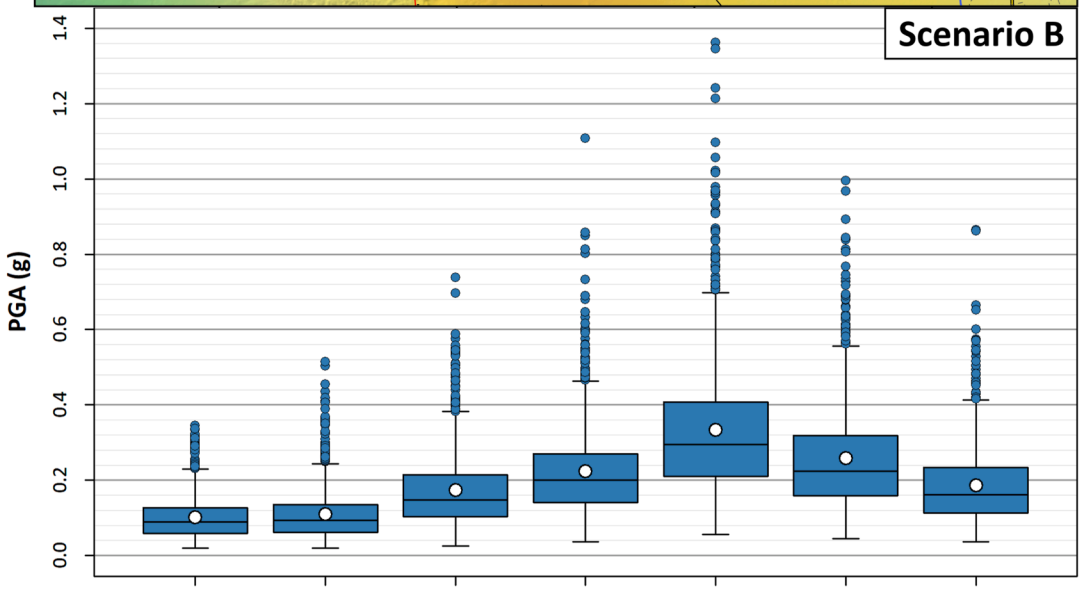

PGA (g)	Nihuil	Reyunos	Valle Grande	San Rafael	Las Malvinas	Villa Atuel	Gral. Alvear
Mean	0.102	0.110	0.174	0.224	0.333	0.259	0.186
Std. dev.	0.059	0.069	0.101	0.121	0.179	0.142	0.104
*Q*1	0.059	0.062	0.103	0.140	0.210	0.158	0.113
Median	0.089	0.094	0.148	0.201	0.295	0.224	0.162
*Q*3	0.127	0.135	0.215	0.270	0.407	0.319	0.234

Fig. 10. Ground motion field for Scenario B expressed as median PGA (g) and anthropic elements. The *p*-*p*' transect corresponds to the cross section in Fig. 12. Below, PGA variability for 1000 realizations with a 99% confidence level in the seven sites of interest, with its corresponding summary table.

6. Discussion

Some points of discussion related to the choice of input parameters for the simulations were already exposed in the methodology section. The present section focuses on discussions that arise from interpreting and analyzing the obtained ground motion fields, bearing in mind the three research questions presented in the Introduction.

6.1. The 1929 LMVA event

The results of this study contribute to the discussion on the source of the 1929 LMVA earthquake. Two hypotheses were tested by modeling the ground motion fields that could have occurred with the Las Malvinas fault as a seismogenic source (Scenario A) and with a deep source east of that fault (Scenario B).

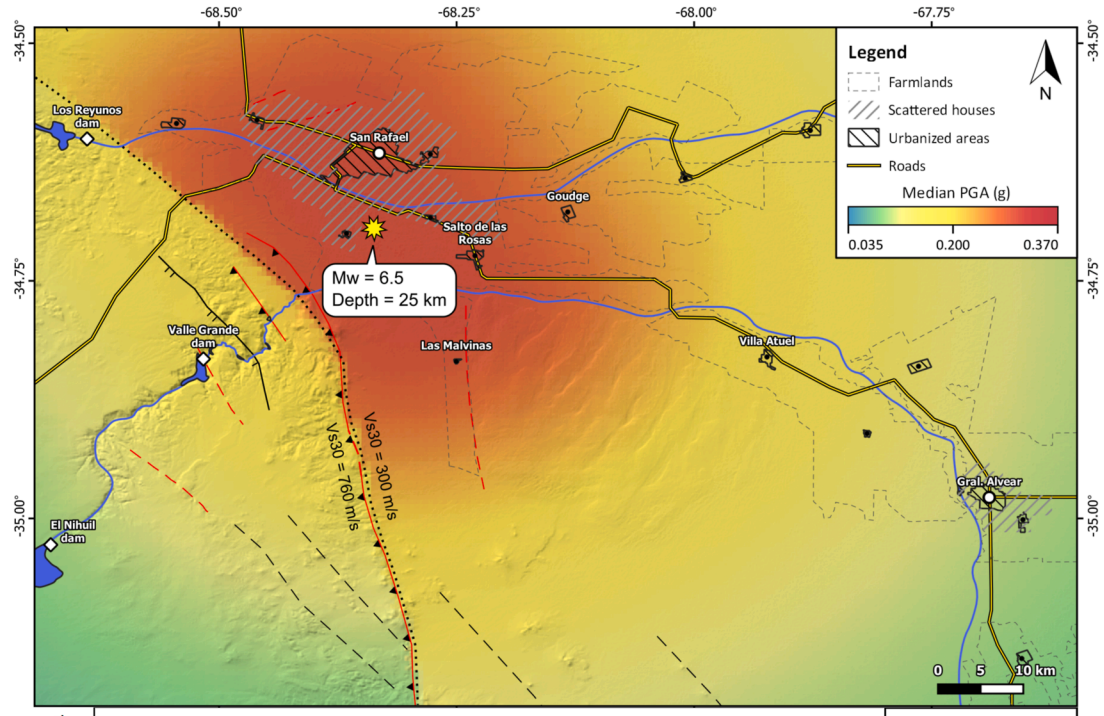

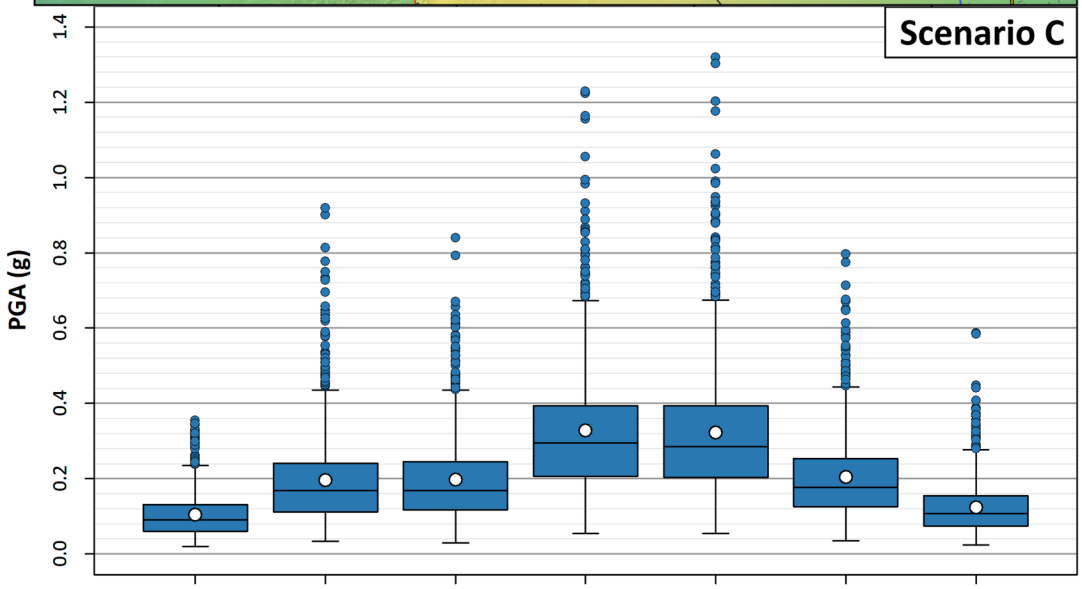

PGA (g)	Nihuil	Reyunos	Valle Grande	San Rafael	Las Malvinas	Villa Atuel	Gral. Alvear
Mean	0.105	0.197	0.198	0.328	0.322	0.205	0.124
Std. dev.	0.060	0.123	0.115	0.174	0.173	0.113	0.070
*Q*1	0.060	0.111	0.117	0.206	0.203	0.125	0.074
Median	0.091	0.168	0.168	0.295	0.285	0.177	0.107
*Q*3	0.131	0.241	0.245	0.394	0.394	0.253	0.155

Fig. 11. Ground motion field for Scenario C expressed as median PGA (g) and anthropic elements. Below, PGA variability for 1000 realizations with a 99% confidence level in the seven sites of interest, with its corresponding summary table.

Considering the Las Malvinas fault as the source carries the advantage that it is an observed fault on the surface with evidence of neotectonic activity [10,11]. However, it carries disadvantages that are highlighted by comparing the results of Scenario A with the destructive effects described in some of the urban settlements (Fig. 9). Even though studies around the world show that the same Mercalli intensity can be related to a wide range of PGA values [63–66], the utter destruction suffered in Villa Atuel would be hard to explain with a median PGA of 0.078 g and a *Q*3 (75% percentile) at 0.112 g (75% of the realizations return a value lower than this). Additionally, the shallow depth of this scenario derives in a stronger attenuation with distance, which produces a PGA with a

Q3 at 0.080 g for General Alvear. The slight damage suffered by that city would be difficult to justify with such a weak shaking intensity.

Comparing the macroseismic estimations with the ground motion field of Scenario B (Fig. 10) shows a better correlation than with the one of Scenario A. Median PGA values of 0.295 and 0.224 g with Q3 at 0.407 and 0.319 g for Las Malvinas and Villa Atuel towns are well inside the range that could cause damage Grade 5 on most Class A buildings. Moreover, even though the PGA at Villa Atuel is lower than at Las Malvinas, the severe damage in the former would be justified by the evidence of liquefaction processes [3,9], a phenomenon that can greatly increase the consequences of ground shaking [46,67,68]. However, a weak point of this simulation is the PGA obtained for San Rafael city (Q1 = 0.140 g; median = 0.201 g; Q3 = 0.270 g). These values seem inconsistent, considering only slight damage was reported. Possible explanations for this are: i) that the depth was overestimated and thus the attenuation was weaker than in reality, where strong shaking could have focused inside a smaller range; ii) that the epicenter was actually located further south; iii) that Vs30 was underestimated, even though tests with up to 450 m/s did not show major changes; iv) that the PGA value in reality was on the lower end of the distribution predicted by the GMPE; v) other site-specific factors like nonlinear behavior of soil sites, which can attenuate ground shaking [69–71].

The meticulous observations made by Lunkenheimer [9] almost a hundred years ago allowed him to point to an epicenter that, in light of the results of Scenario B, is quite compatible with the evidence. However, given that he lacked the tools to estimate the source depth, the present study tries to fill that gap by adding our modern information through the criteria mentioned in previous sections. The 25 km deep hypocenter is consistent with the nearby low-magnitude seismicity captured by local networks and would be plausible with a NE-dipping major blind thrust as the one proposed by Olivar et al. [22] (Fig. 12). In that study, the authors explored the tectonic implications of that alternative model for the San Rafel Block and compared it with other broken foreland scenarios where uplift occurs with a different strike and vergence than in the neighboring orogen, possibly due to inherited crustal discontinuities (e.g., the Laramide ranges in the Rocky Mountains of North America [72–75], and the Sierras Pampeanas developed over the Chilean-Pampean flat slab subduction segment [76–79]). In the present discussion, this structural model is also a better fit for the seismogenic source under investigation, as opposed to the Las Malvinas fault. It is important to note that, even though Branellec et al. [11] considered the Las Malvinas fault as a potential seismic source of the 1929 LMVA event, they also pointed out that the surface deformation observed near the fault trace could be a secondary and shallow effect detached from the deep-seated blind thrusting that would host the seismic activity. Our results favor the second statement and provide stronger support for the epicenter location suggested by Lunkenheimer [9].

Even though the simulations deliver new information on the present discussion, it is clear that further studies, specifically about site conditions, would be needed to trace back the real hypocenter with more precision. However, narrowing down the options allows constraining the scenarios for future possible events of similar characteristics, which eventually could be input into a probabilistic seismic hazard analysis in a more data and resource-rich study.

6.2. Ground shaking at sites of interest

The three simulations provide a range of ground motion estimations for better and worse case scenarios at the seven sites of interest. These give a general idea of what PGA to expect if the MHE was repeated but with different hypocenter positions. Q3 is mentioned together with the median PGA, since it represents a more conservative approach.

- El Nihuil dam: the highest values take place in Scenario A, reaching a median of 0.168 g with a Q3 at 0.241 g. In the other scenarios, the median PGA lies below 0.100 g.
- Los Reyunos dam: it presents the same statistical values as El Nihuil dam, but given Scenario C. No other scenarios return a median PGA over 0.100 g.
- Valle Grande dam: median PGA rises up to 0.313 g with Q3 = 0.455 g in Scenario A. The other two scenarios return approximately half these values.
- San Rafael: Scenario C returns a median PGA of 0.295 g with 75% of realizations under 0.394 g. The more distant epicenter given by Scenario A gives a median of 0.133 g.
- Las Malvinas: PGA values are relatively high in the three scenarios. The highest median PGA is 0.295 g with Q3 = 0.407 g in Scenario B.
- Villa Atuel: median PGA rises to 0.224 g with Q3 at 0.319 g in Scenario B, while Scenario C shows a considerable median PGA of 0.177 g with Q3 at 0.253 g.
- General Alvear: the highest values correspond to Scenario B, with a median of 0.162 g and Q3 = 0.234 g.

It is worth noting that PGA values at the dams may be very overestimated, since we applied a Vs30 on the lowest end for rock sites ("soil type B", 760 m/s). For this kind of key facility, it is better to adopt a conservative value rather than a potentially underestimated one. However, in the case of El Nihuil and Valle Grande dams, the highest accelerations take place in Scenario A, which, according to the present study, would not be representative of the 1929 LMVA earthquake (MHE). Nonetheless, the simulation is still relevant because studies on the neotectonics and structural features of the Las Malvinas and Cerro Negro faults estimated a seismogenic potential of up to *M*6.9 and *M*6.4 respectively, mostly based on the surface extension of the fault traces and the Wells and Coppersmith relationships [11,40]. Recurrence times of 520 and 440 years were calculated based on the slip rates of these faults. Thus, a fourth scenario that remains untested would be similar to Scenario A but with an epicenter selected northward, very close to the Valle Grande dam, following the orientation of the Cerro Negro fault (immediately north of the Las Malvinas fault). Keeping the same source depth and magnitude, that dam would be exposed to a median PGA of around 0.370 g in such a case.

Villa Atuel constitutes another special case since it is the only town where descriptions of liquefaction effects were reported, caused by a shallow phreatic level at 1 m depth [9]. This effect would increase the damage considerably if a similar earthquake took place [46,67,68]. However, that phreatic level was described as artificially generated by constant irrigation. It is highly likely that this condition changed after almost a hundred years, which demands new studies on the current site conditions.

6.3. Comparison to other studies and building codes

The next point of discussion is how these PGA values compare to previous studies and existing building codes. Fig. 5 shows the PGA values calculated by probabilistic studies of regional to global scales. It is difficult to make a direct comparison between the results of our deterministic study and those of a probabilistic one, since the former points towards extreme scenarios that most probably exceed the 475-return period usually reported in hazard

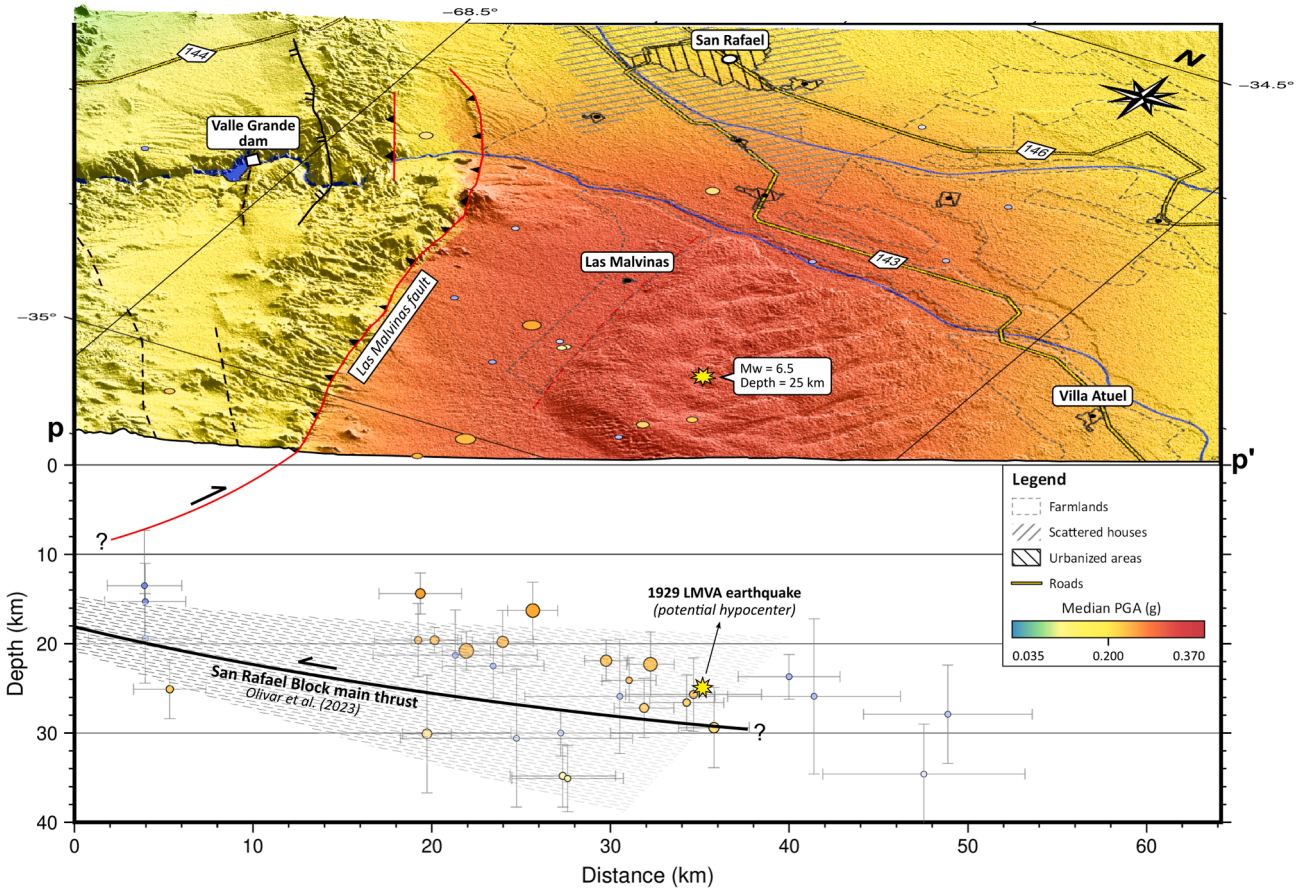

Fig. 12. Cross-section at the *p*-*p*' transect shown in Fig. 10, illustrating the position of the 1929 LMVA hypocenter proposed in Scenario B in relation to the seismicity recorded by local networks and to the potential San Rafael Block main thrust proposed in Olivar et al. [22]. Hypocenter symbols follow the same code as in Fig. 4.

maps. For scenario A and others potentially triggered by the Las Malvinas and Cerro Negro fault, the comparison is more robust taking into account the return periods of 520 and 440 years for $M > 6$ events estimated by Branellec et al. [11], which are close to the standard 475-year return period. But scenarios triggered by blind faults preclude the possibility of approximating a return period through slip rate or paleoseismology studies. The relatively low seismicity ratio of the area, with very limited $M > 4$ events registered in catalogs, also hinders the capability of estimating a magnitude-recurrence relationship to use in probabilistic analysis. However, a worthy discussion is whether the regional and global probabilistic studies already cover the scenarios presented here and, further on, whether current building codes are already suitable even for extreme scenarios.

First, according to the GEM hazard map, the area is divided into three zones, which span a PGA of 0.13–0.40 with a 475-year return period (Fig. 5a [42]). This map was derived from global earthquake data, using reference rock conditions for the whole area, intended for a first-order approximation of global earthquake hazard. Interestingly, the area with the highest hazard is located on the eastern side of the study region, including General Alvear City, which was one of the least affected sites in the simulations done by the present study and during the 1929 LMVA event. This is probably explained by the fact that their catalog locates the event displaced to the east with respect to the epicenter supported here and proposed by Lunkenheimer [9] (Fig. 4). This may have had a great impact on their calculations, resulting in exaggerated estimations of PGA for an area where local networks show little to no seismicity [22,41].

In the old seismic zoning map reported by INPRES, most of the sites of interest fall inside the zone with PGA = 0.25 g for a 475 return period (Fig. 5b). El Nihuil Dam and General Alvear are left outside, with a PGA of 0.18 g. This was rectified in the recent new map, which shows the whole area over 0.18 g and the west side between 0.25 and 0.35 g, including San Rafael, Las Malvinas, and the dams. This new map is almost exactly opposite to the GEM hazard map, where the highest PGA is not observed on the east side but rather on the west one. All of our highest median PGA values (summarized in the previous section), considering the three scenarios for each of the seven sites, lie within the ranges established by the new map. This indicates that with the results obtained by INPRES for a return period of 475 years, the sites should be covered for rarer and extreme events like the 1929 LMVA earthquake. Only if we consider Q3 instead of the median, PGA reported by INPRES's new map is exceeded by our simulations in three of the seven sites: Valle Grande dam, San Rafael and Las Malvinas.

Leaving aside site- and building-specific response spectra, this analysis suggests that if building codes enforced in the area followed INPRES's new hazard map, exposed elements would remain within safe limits even for an event such as the MHE. However, the current building codes are based on the old map [14], which recommends seismic action for a maximum of 0.25 g instead of 0.35 g for most of the sites of interest. This would not be a problem for the dams since the codes also recommend a multiplication factor of 1.4 for seismic action in energy facilities. More specifically, dams are expected to be designed to withstand the ground motions of the safety evaluation earthquake (SEE), which refers to the maximum

believable earthquake or worst-case scenario (see Ref. [80] for a review). Instead, the main problem would be focused on cities and towns where buildings may not be prepared for PGA exceeding 0.25 g.

Given these considerations, the strong recommendation made by this study is that a full reassessment of the building stock should be carried out, focusing on Class A and B vulnerability buildings and updating the seismic action to resist the updated hazard values reported by INPRES. This would be sufficient to account for events comparable to the MHE, as well as ~500-year recurrence events on the Las Malvinas and Cerro Negro faults, as simulated here.

7. Conclusions

Three earthquake scenarios were simulated using OpenQuake for the region surrounding San Rafael and General Alvear cities in Mendoza province. Two of them had the goal of recreating the maximum historical earthquake that took place in 1929 and destroyed the towns of Las Malvinas and Villa Atuel. The last one was proposed as a worse-case scenario for the city of San Rafael.

Model input parameters were narrowed down using different criteria and assumptions aided by previous studies. The variable that showed the greatest effect on the attenuation of PGA with distance from the source was Vs30. Thus, two different values were used for rock and soil sites. PGA variation did not show great dependency with hypocenter depth and fault dip, inside a plausible range for the modeled faults.

Our results, in view of descriptions of the 1929 historic earthquake's effects on anthropic elements found in the literature and online newspaper articles, revealed that the epicenter could have probably been located around 13 km southeast of Las Malvinas town, supporting the estimations of Lunkenheimer [9]. Locations displaced to the east reported by global catalogs from ISC and USGS, and to the west suggested by Costa et al. and Branellec et al. [10,11], were discarded based on the characteristics of the macroseismic field. Instead of considering the shallow Las Malvinas fault as the seismogenic source, we propose a ~25 km deep hypocenter nucleated in the potential deep-seated, northeast-dipping blind structure that uplifts the San Rafael Block according to our previous study based on seismic and gravimetric data [22].

One thousand realizations of each scenario in seven specific sites (three hydroelectric dams, San Rafael and General Alvear cities, and Las Malvinas and Villa Atuel towns) allowed the calculation of the full distribution of possible PGA levels. All sites show median PGA values below 0.315 g and 75% of the realizations below 0.460 g. The median values and most of the Q3 values are well inside the range reported by INPRES's recent country-wide probabilistic hazard map for a return period of 475 years.

The current building codes by INPRES were based on old estimations, with PGA values that fall beneath both the probabilistic results of their new hazard study and the deterministic results for magnitude 6.5 scenarios presented here. Hence, we recommend an update of the codes and a reassessment of the building stock to comply with the new hazard map, which would also account for rare events such as the 1929 earthquake. Further studies on magnitude-recurrence relationships, site conditions, and local probabilistic hazards are also encouraged.

CRediT authorship contribution statement

Julián Olivar: Writing – original draft, Visualization, Software, Methodology, Investigation, Formal analysis, Data curation, Conceptualization. **Silvina Nacif:** Writing – review & editing, Validation, Supervision. **Andrés Folguera:** Writing – review & editing, Validation, Supervision.

Declaration of competing interest

The authors declare that they have no known competing financial interests or personal relationships that could have appeared to influence the work reported in this paper.

The author Andrés Folguera is an Associate Editor for *Geodesy and Geodynamics* and was not involved in the editorial review or the decision to publish this article.

Acknowledgements

This project was carried out within the framework of the Specialisation Certificate for the Assessment and Management of Geological and Climate-related Risk of the University of Geneva (CERG-C) (https://www.unige.ch/sciences/terre/CERG-C/). We would like to thank Corine Frischknecht, Blaise Duvernay (University of Geneva) and Donat Fäh (ETH Zurich) for their support during the program and their contribution to the project.

References

[1] J.C. Castano, J.L. Zamarbide, Fuentes Sismogénicas, Sismicidad Histórica y peligro sísmico en la Zona Centro-Oeste Argentina, Rev. Geofisc. 34 (1991) 17–38.
[2] G.E. Tello, Sismicidad histórica entre los 32o 30' - 36o lat. sur y los 68o- 69o 30' long. oeste, provincia de Mendoza, Argentina, Rev. Geogr. Venez. 44 (1) (2003) 125–141.
[3] L. Perucca, A. Pérez, C. Navarro, Fenómenos de licuefacción asociados a terremotos históricos. Su análisis en la evaluación del peligro sísmico en la Argentina, Rev. Asoc. Geológica Argent. 61 (4) (Dec. 2006) 567–578.
[4] L.D. Jaime, A.I. García, La sismicidad en el NOA (República Argentina). Una visión histórico-geográfica, Rev. Geogr. (146) (2009) 205–231.
[5] INPRES, Terremotos históricos ocurridos en la República Argentina. http://contenidos.inpres.gob.ar/sismologia/historicos. (Accessed 29 January 2026).
[6] P. Loos, Estudios de sismología. Los movimientos sísmicos de Mendoza, Ministerio de Agricultura, 1907. Sección Geología.
[7] S. Schmidt, R. Hetzel, F. Mingorance, V.A. Ramos, Coseismic displacements and Holocene slip rates for two active thrust faults at the mountain front of the Andean precordillera (~33°S), Tectonics 30 (5) (Oct. 2011), https://doi.org/10.1029/2011TC002932, 2011TC002932.
[8] International Seismological Centre, ISC-GEM earthquake catalogue, 2023, https://doi.org/10.31905/D808B825.
[9] F. Lunkenheimer, El terremoto sudmendocino del 30 de Mayo de 1929, in: Contribuciones Geofísicas del Observatorio Astronómico de la Universidad de La Plata, Tomo III, N°2, La Plata, Argentina, 1930, pp. 89–143.
[10] C. Costa, H. Cisneros, J. Salvarredi, A. Galluci, La neotectónica del margen oriental del bloque de San Rafael: nuevas consideraciones, Asoc. Geológica Argent. Ser. Publ. Espec. 6 (2006) 33–40.
[11] M. Branellec, B. Nivière, J.-P. Callot, V. Regard, J.-C. Ringenbach, Evidence of active shortening along the eastern border of the San Rafael basement block: characterization of the seismic source of the Villa Atuel earthquake (1929), Mendoza province, Argentina, Geol Mag 153 (5–6) (Sep. 2016) 911–925, https://doi.org/10.1017/S0016756816000194.
[12] H. Bastías, G. Tello, L. Perucca, J. Paredes, V. Ramos, Peligro sísmico y neotectónica, in: Geología de la provincia de Mendoza: XII Congreso Geologico Argentino, Relatorio, 1993, pp. 645–658.
[13] INPRES, "Zonificación Sísmica de Argentina." Accessed: January. 29, 2026. [Online]. Available:http://contenidos.inpres.gob.ar/acelerografos/Reglamentos#Zonificaci%C3%B3n%20S%C3%ADsmica.
[14] INPRES, Reglamento Argentino para Construcciones Sismorresistentes ("INPRES-CIRSOC 103"), Buenos Aires, Argentina: INTI, 2018.
[15] International Seismological Centre, ISC bulletin, 2022, https://doi.org/10.31905/D808B830.
[16] A.M. Dziewonski, T.-A. Chou, J.H. Woodhouse, Determination of earthquake source parameters from waveform data for studies of global and regional seismicity, J Geophys Res Solid Earth 86 (B4) (Apr. 1981) 2825–2852, https://doi.org/10.1029/JB086iB04p02825.
[17] G. Ekström, M. Nettles, A.M. Dziewoński, The global CMT project 2004–2010: centroid-Moment tensors for 13,017 earthquakes, Phys Earth Planet Inter 200–201 (Jun. 2012) 1–9, https://doi.org/10.1016/j.pepi.2012.04.002.
[18] INPRES, Actualización del Mapa de Peligrosidad Sísmica de Argentina. http://contenidos.inpres.gob.ar/actualizacion_mapa. (Accessed 29 January 2026).
[19] G. Sánchez, Estudio de peligrosidad sísmica para la República Argentina, Universidad Nacional de San Juan, San Juan, Argentina, 2022. PhD thesis.

[20] G. Sánchez, A. Giuliano, Nuevo mapa de amenaza sísmica de Argentina. presented at the XXVIII Jornadas Argentinas de Ingeniería Estructural, 2024. Buenos Aires, Argentina.
[21] A.B. Balbi, M. Coppolecchia, J.A. Oliva, M.A. Rosas, "Diagnóstico de la Peligrosidad Geológica de la Ciudad de San Rafael, Provincia de Mendoza, Argentina," Ministerio de Producción y Trabajo, Servicio Geológico Minero Argentino. Instituto de Geología y Recursos Minerales, 2019. https://repositorio.segemar.gov.ar//handle/308849217/2848. (Accessed 29 January 2026).
[22] J. Olivar, S. Nacif, M. Giménez, B. Heit, L. Fennell, A. Folguera, Structure and seismogenic activity of the broken foreland to the south of the chilean-pampean flat subduction zone: the San Rafael Block, J South Am Earth Sci 124 (Apr. 2023) 104260, https://doi.org/10.1016/j.jsames.2023.104260.
[23] M. Pagani, et al., OpenQuake engine: an open hazard (and risk) software for the global earthquake model, Seismol Res. Lett. 85 (3) (May 2014) 692–702, https://doi.org/10.1785/0220130087.
[24] P. Criado Roque, Bloque de San Rafael, in: Geología regional Argentina, Academia Nacional de Ciencias, 1972, pp. 288–295.
[25] C.A. Cingolani, M. Manassero, P. Abre, Composition, provenance, and tectonic setting of Ordovician siliciclastic rocks in the San Rafael block: southern extension of the Precordillera crustal fragment, Argentina, J South Am Earth Sci 16 (1) (May 2003) 91–106, https://doi.org/10.1016/S0895-9811(03)00021-X.
[26] T.E. Jordan, B.L. Isacks, R.W. Allmendinger, J.A. Brewer, V.A. Ramos, C.J. Ando, Andean tectonics related to geometry of subducted nazca plate, Geol Soc Am Bull 94 (3) (1983) 341, https://doi.org/10.1130/0016-7606(1983)94<341:ATRTGO>2.0.CO;2.
[27] V.A. Ramos, E.O. Cristallini, D.J. Pérez, The Pampean flat-slab of the Central Andes, J South Am Earth Sci 15 (1) (Apr. 2002) 59–78, https://doi.org/10.1016/S0895-9811(02)00006-8.
[28] S.M. Kay, W.M. Burns, P. Copeland, O. Mancilla, Upper Cretaceous to Holocene magmatism and evidence for transient Miocene shallowing of the Andean subduction zone under the northern Neuquén Basin, in: Evolution of an andean margin: a tectonic and magmatic view from the andes to the Neuque'n Basin (35°-39°S lat), Geological Society of America, 2006, https://doi.org/10.1130/2006.2407(02).
[29] A. Folguera, et al., Retroarc volcanism in the northern San Rafael Block (34°–35°30'S), southern Central Andes: occurrence, age, and tectonic setting, J. Volcanol. Geoth. Res. 186 (3–4) (Oct. 2009) 169–185, https://doi.org/10.1016/j.jvolgeores.2009.06.012.
[30] M. Anderson, P. Alvarado, G. Zandt, S. Beck, Geometry and brittle deformation of the subducting Nazca Plate, Central Chile and Argentina, Geophys J Int 171 (1) (Oct. 2007) 419–434, https://doi.org/10.1111/j.1365-246X.2007.03483.x.
[31] S. Nacif, E.G. Triep, S.L. Spagnotto, E. Aragon, R. Furlani, O. Álvarez, The flat to normal subduction transition study to obtain the Nazca plate morphology using high resolution seismicity data from the Nazca plate in Central Chile, Tectonophysics 657 (Aug. 2015) 102–112, https://doi.org/10.1016/j.tecto.2015.06.027.
[32] E.G. Sepúlveda, F.W. Carpio, M.C. Regairaz, M. Zárate, J.C.M. Zanettini, H.A. Leanza, Hoja Geológica 3569-II San Rafael, Boletín 321, Servicio Geológico Minero Argentino. Instituto de Geología y Recursos Minerales, Buenos Aires, Argentina, 2007 [Online]. Available: https://repositorio.segemar.gov.ar//handle/308849217/181. (Accessed 29 January 2026).
[33] E.G. Sepúlveda, A. Bermúdez, O. Bordonaro, D. Delpino, H.S. Mallimacci, H.A. Leanza, Hoja Geológica 3569-IV embalse El Nihuil, Boletín 268, Servicio Geológico Minero Argentino. Instituto de Geología y Recursos Minerales, Buenos Aires, Argentina, 2007 [Online]. Available: https://repositorio.segemar.gov.ar//handle/308849217/117. (Accessed 29 January 2026).
[34] SEGEMAR, "Catálogo de Datos Abiertos Geoespaciales, Deformaciones Cuaternarias 250k." Sistema de Información Geológica Ambiental Minera (SIGAM), 2025. https://sigam.segemar.gov.ar/mapstore/#/viewer/458. (Accessed 29 January 2026).
[35] D. Richarte, M. Lupari, A. Pesce, S. Nacif, M. Gimenez, 3-D crustal-scale gravity model of the San Rafael Block and payenia volcanic province in Mendoza, Argentina, Geosci Front 9 (1) (Jan. 2018) 239–248, https://doi.org/10.1016/j.gsf.2017.03.004.
[36] M.S. Morales Volosín, C. Prezzi, C. Risso, Relationships between Payenia volcanism and deep-seated structural controls: insights from geophysical methods at Nevado volcanic field, Mendoza, Argentina, J South Am Earth Sci 116 (Jun. 2022) 103779, https://doi.org/10.1016/j.jsames.2022.103779.
[37] C. Lucero, J. Paredes, Fallamiento rumbo-deslizante en la falla Aisol, Bloque de San Rafael, Mendoza, in: *Actas*, Salta, Argentina, 1999, pp. 263–266.
[38] M.L. Peñalva, M.L. Vélez, Análisis estructural de la deformación cenozoica, sector sur Bloque de San Rafael, Mendoza (34o 50'- 35o S, 68o 27'- 68o 37' O), in: *Actas*, La Plata, Argentina, 2005.
[39] H. Neilson, Landform evolution in the Southern central andes: the major mechanisms of formation of the Santa Isabel escarpment, 34° to 38°S, argentina," degree thesis, Dalhousie University, Halifax, Nova Scotia, Canada, 2007.
[40] D.L. Wells, K.J. Coppersmith, New empirical relationships among magnitude, rupture length, rupture width, rupture area, and surface displacement, Bull Seismol Soc Am 84 (4) (Aug. 1994) 974–1002, https://doi.org/10.1785/BSSA0840040974.
[41] M.N. Lupari, et al., Sismicidad localizada en la zona del Bloque San Rafael, Argentina, Rev. Mex. Ciencias Geol. 32 (2) (Aug. 2015) 190–202.
[42] K. Johnson, et al., Global seismic hazard map, Zenodo, Oct. 13, 2023, https://doi.org/10.5281/ZENODO.8409647.
[43] S.A. Otta, Lineamientos ambientales para el Ordenamiento Territorial de zonas periurbanas. San Rafael, Mendoza, Universidad Nacional de Cuyo, Mendoza, Argentina, 2014. Degree thesis.
[44] G. Cuitiño, R. Rotondaro, A. Esteves, G. Maldonado, Clasificación y estudio experimental del comportamiento de suelos mendocinos para la construcción de quinchas, Av. En Energ. Renov. Medio Ambiente 14 (2010).
[45] P. Alvarado, R. Christiansen, S.D. Gregori, M. Saez, Evidence of site amplification from ground motion of the last two large crustal earthquakes in central-western Argentina, Nat Hazards 102 (3) (Jul. 2020) 1011–1031, https://doi.org/10.1007/s11069-020-03943-8.
[46] European macroseismic scale 1998: EMS-98, in: G. Grünthal (Ed.), Cahiers du Centre européen de géodynamique et de séismologie, no. v. 15, second ed., European Seismological Commission, Subcommission on Engineering Seismology, Working Group Macroseismic scales, Luxembourg, 1998.
[47] M. Branellec, B. Nivière, J.-P. Callot, J.-C. Ringenbach, Mechanisms of basin contraction and reactivation in the basement-involved Malargüe fold-and-thrust belt, Central Andes (34–36°S), Geol Mag 153 (5–6) (Sep. 2016) 926–944, https://doi.org/10.1017/S0016756816000315.
[48] S.M. Saurina, M.E. Quiles, B. Faro, B. Bragoni, A.M. Mateu, Pioneros de Villa Atuel Mendoza. Recuperación del patrimonio a cien años de su fundación. Protagonismo del agua, San Rafael, Mendoza, Argentina (2012).
[49] M. Izuel, "El fatal terremoto de 1929 que sacudió y cambió San Rafael," Diario Uno. Accessed: January. 29, 2026 [Online]. Available:https://www.diariouno.com.ar/san-rafael/fatal-terremoto-1929-sacudio-cambio-san-rafael-19082015_B1M96K_f1B.
[50] A.B. Rodríguez, Análisis de la peligrosidad sísmica en la región de la Cuenca Neuquina, Universidad Nacional de La Plata, La Plata, Argentina, 2022. Degree thesis.
[51] J.P. Stewart, et al., Selection of ground motion prediction equations for the global earthquake model, Earthq Spectra 31 (1) (Feb. 2015) 19–45, https://doi.org/10.1193/013013EQS017M.
[52] N.A. Abrahamson, W.J. Silva, R. Kamai, Summary of the ASK14 ground motion relation for active crustal regions, Earthq Spectra 30 (3) (Aug. 2014) 1025–1055, https://doi.org/10.1193/070913EQS198M.
[53] D.M. Boore, J.P. Stewart, E. Seyhan, G.M. Atkinson, NGA-West2 equations for predicting PGA, PGV, and 5% damped PSA for shallow crustal earthquakes, Earthq Spectra 30 (3) (Aug. 2014) 1057–1085, https://doi.org/10.1193/070113EQS184M.
[54] K.W. Campbell, Y. Bozorgnia, NGA-West2 ground motion model for the average horizontal components of PGA, PGV, and 5% damped linear acceleration response spectra, Earthq Spectra 30 (3) (Aug. 2014) 1087–1115, https://doi.org/10.1193/062913EQS175M.
[55] B.S.-J. Chiou, R.R. Youngs, Update of the chiou and youngs NGA model for the average horizontal component of peak ground motion and response spectra, Earthq Spectra 30 (3) (Aug. 2014) 1117–1153, https://doi.org/10.1193/072813EQS219M.
[56] I.M. Idriss, An NGA-West2 empirical model for estimating the horizontal spectral values generated by shallow crustal earthquakes, Earthq Spectra 30 (3) (Aug. 2014) 1155–1177, https://doi.org/10.1193/070613EQS195M.
[57] J. Douglas, Ground motion prediction equations 1964–2021, Department of Civil and Environmental Engineering University of Strathclyde, Glasgow, United Kingdom, 2022.
[58] E.M. Rathje, S. Navidi, Identification of site parameters that improve predictions of site amplification, University of California, Berkeley, USA, 2013. Report 18.
[59] D.J. Wald, T.I. Allen, Topographic slope as a proxy for seismic site conditions and amplification, Bull Seismol Soc Am 97 (5) (Oct. 2007) 1379–1395, https://doi.org/10.1785/0120060267.
[60] T.I. Allen, D.J. Wald, On the use of high-resolution topographic data as a proxy for seismic site conditions (VS30), Bull Seismol Soc Am 99 (2A) (Apr. 2009) 935–943, https://doi.org/10.1785/0120080255.
[61] D.C. Heath, D.J. Wald, C.B. Worden, E.M. Thompson, G.M. Smoczyk, A global hybrid Vs30 map with a topographic slope–based default and regional map insets, Earthq Spectra 36 (3) (Aug. 2020) 1570–1584, https://doi.org/10.1177/8755293020911137.
[62] R. Zaccarelli, G. Weatherill, D. Bindi, A. Strollo, F. Cotton, eGSIM: a web service for selecting and testing ground shaking models in Europe, in: Geophysical research abstracts, 2018. Vienna, Austria.
[63] D.J. Wald, V. Quitoriano, T.H. Heaton, H. Kanamori, Relationships between peak ground acceleration, peak ground velocity, and modified Mercalli intensity in California, Earthq Spectra 15 (3) (Aug. 1999) 557–564, https://doi.org/10.1193/1.1586058.
[64] L. Linkimer, Relationship between peak ground acceleration and modified Mercalli intensity in Costa Rica, Rev. Geol. Am. Cent. (38) (2008) 81–94.
[65] G.-A. Tselentis, L. Danciu, Empirical relationships between modified Mercalli intensity and engineering ground-motion parameters in Greece, Bull Seismol Soc Am 98 (4) (Aug. 2008) 1863–1875, https://doi.org/10.1785/0120070172.
[66] A.A. Gomez-Capera, M. D'Amico, G. Lanzano, M. Locati, M. Santulin, Relationships between ground motion parameters and macroseismic intensity for Italy, Bull Earthq Eng 18 (11) (Sep. 2020) 5143–5164, https://doi.org/10.1007/s10518-020-00905-0.

[67] K. Ishihara, Liquefaction and flow failure during earthquakes, Geotechnique 43 (3) (Sep. 1993) 351–451, https://doi.org/10.1680/geot.1993.43.3.351.
[68] Y. Huang, M. Yu, Review of soil liquefaction characteristics during major earthquakes of the twenty-first century, Nat Hazards 65 (3) (Feb. 2013) 2375–2384, https://doi.org/10.1007/s11069-012-0433-9.
[69] E.H. Field, et al., Nonlinear site response: where we're at (A report from a SCEC/PEER seminar and workshop), Seismol Res. Lett. 69 (3) (May 1998) 230–234, https://doi.org/10.1785/gssrl.69.3.230.
[70] R.J. Archuleta, L.F. Bonilla, D. Lavallee, Nonlinearity in observed and computed accelerograms, in: The proceedings of the 12th world conference on earthquake engineering, Aston Koedyk Ldt, Auckland, New Zealand, 2000, p. 7.
[71] V. Poggi, D. Fäh, Guidelines and strategies for seismic microzonation in Switzerland, ETH Zurich (2016), https://doi.org/10.3929/ETHZ-A-010735479.
[72] S.B. Smithson, J. Brewer, S. Kaufman, J. Oliver, C. Hurich, Nature of the wind river thrust, Wyoming, from COCORP deep-reflection data and from gravity data, Geology 6 (11) (1978) 648, https://doi.org/10.1130/0091-7613(1978)6<648:NOTWRT>2.0.CO;2.
[73] D.S. Stone, Basement-involved thrust-generated folds as seismically imaged in the subsurface of the central rocky Mountain foreland, in: Geological society of America special papers, vol. 280, Geological Society of America, 1993, pp. 271–318, https://doi.org/10.1130/SPE280-p271.
[74] P.G. DeCelles, Late Jurassic to Eocene evolution of the Cordilleran thrust belt and foreland basin system, Western U.S.A. Am J Sci 304 (2) (Feb. 2004) 105–168, https://doi.org/10.2475/ajs.304.2.105.
[75] W.A. Yonkee, A.B. Weil, Tectonic evolution of the sevier and laramide belts within the North American Cordillera orogenic system, Earth Sci. Rev. 150 (Nov. 2015) 531–593, https://doi.org/10.1016/j.earscirev.2015.08.001.
[76] F. González Bonorino, Algunos problemas geológicos de las Sierras Pampeanas, Rev. Asoc. Geológica Argent. 5 (3) (Jul. 1950) 6–110.
[77] T.E. Jordan, R.W. Allmendinger, The Sierras Pampeanas of Argentina; a modern analogue of rocky Mountain foreland deformation, Am J Sci 286 (10) (Dec. 1986) 737–764, https://doi.org/10.2475/ajs.286.10.737.
[78] A. Introcaso, A. Lion, V.A. Ramos, La estructura profunda de las Sierras de Córdoba, Rev. Asoc. Geológica Argent. 42 (1–2) (Jun. 1987) 177–187.
[79] V.A. Ramos, E.O. Cristallini, D.J. Pérez, The Pampean flat-slab of the central Andes, J South Am Earth Sci 15 (1) (Apr. 2002) 59–78, https://doi.org/10.1016/S0895-9811(02)00006-8.
[80] M. Wieland, Safety aspects of sustainable storage dams and earthquake safety of existing dams, Engineering 2 (3) (Sep. 2016) 325–331, https://doi.org/10.1016/J.ENG.2016.03.011.



Dr. Julián Andrés Olivar, is a Geology PhD and teaching assistant at University of Buenos Aires. His doctoral work focused on crustal seismicity and neotectonics in the Central Andes of Argentina. He is currently a CONICET postdoctoral researcher specializing in volcano seismology.